

Three-dimensional pattern formation, multiple homogeneous soft modes, and nonlinear dielectric electroconvection

Axel G. Rossberg

Department of Physics, Kyoto University, Kyoto 606-8502, Japan

<http://www.rossberg.net/ag>

(submitted to PRE)

Patterns forming spontaneously in extended, three-dimensional, dissipative systems are likely to excite several homogeneous soft modes (\approx hydrodynamic modes) of the underlying physical system, much more than quasi one- and two-dimensional patterns are. The reason is the lack of damping boundaries. This paper compares two analytic techniques to derive the pattern dynamics from hydrodynamics, which are usually equivalent but lead to different results when applied to multiple homogeneous soft modes. Dielectric electroconvection in nematic liquid crystals is introduced as a model for three-dimensional pattern formation. The 3D pattern dynamics including soft modes are derived. For slabs of large but finite thickness the description is reduced further to a two-dimensional one. It is argued that the range of validity of 2D descriptions is limited to a very small region above threshold. The transition from 2D to 3D pattern dynamics is discussed. Experimentally testable predictions for the stable range of ideal patterns and the electric Nusselt numbers are made. For most results analytic approximations in terms of material parameters are given.

45.70.Qj, 47.20.Ky 61.30.Gd

I. INTRODUCTION

Spontaneous formation of spatially periodic structures on a homogeneous background is ubiquitous in nature, fascinating to look at, and often hard to understand in detail. The periodic structures are almost never ideal. Irregularities may be generated in the transient after the pattern formation is initiated and anneal after some time. Or, in particular in dissipative systems far from equilibrium, they may be the result of an instability of the regular, spatially periodic state itself, then often leading to a state which exhibits persistent spatio-temporally chaotic dynamics. In some systems this is the case arbitrary close to the threshold of pattern formation in control parameter space. With the help of reduced descriptions like phase-diffusion and Ginzburg-Landau like amplitude equations, which are to some extent universal (i.e., independent of physical details), several phenomena associated with these deviations from the simple periodic structure can be explained [1].

For mostly practical reasons, experimental and theoretical research on pattern formation and dynamics has concentrated on quasi one- or two-dimensional systems, but most of the results obtained should have a direct correspondence also in genuinely three dimensional patterns. By a genuinely three dimensional pattern (below simply 3D pattern) I do here mean a spatially periodic structure for which (i) the spatial period(s) are *not* determined by the spatial extension of the sample (referred to as the class of patterns formed by “competing interaction” in Ref. [1]) *and* (ii) for which the spatial extension of the sample is in all directions large compared to the period(s) of the pattern. This is a stronger conception of a “3D pattern” than the one used in Refs. [2,3], which is

based only on (ii).

Additional complications in 3D patterns, as compared to 1D or 2D patterns, arise from the structure and dynamics of defects (dislocations as well as disclinations), which are point like in 2D but line like in 3D. The implications for dissipative, nonpotential systems, mainly those described by the complex Ginzburg-Landau equation, have been addressed by several authors [4–9]. But there is another particularity of 3D patterns, which has so far found little attention: the massive occurrence of *homogeneous soft modes*, which couple to the pattern and can drastically change its dynamics.

By homogeneous soft modes I mean marginally stable or slowly decaying homogeneous or long-wavelength perturbations of the homogeneous basic state from which the pattern arises. In the abstract sense of the word, they are hydrodynamic modes of the basic state. But for the sake of clarity the terms “hydrodynamic mode” and “hydrodynamics” shall here be reserved for slowly relaxing deviations from the *thermodynamic* equilibrium in an unbounded, homogeneous medium, and their dynamics (e.g., the velocity field in a convective flow is a hydrodynamic variable). The pattern-forming basic state is itself a non-equilibrium state. Thus, although there is some correspondence between homogeneous soft modes and hydrodynamic modes (in the narrow sense), the notions are not identical.

As it has become clear by the investigation of several 1D and 2D model systems, homogeneous soft modes are the key for understanding many of the phenomena occurring at, or close to, the onset of pattern formation. The most prominent example is the mode associated with a homogeneous perturbation of the pressure field in Rayleigh-Bénard convection which leads to a “singular mean flow”. It is worth noticing that, since it is usu-

ally possible to construct self-consistent amplitude equations which do *not* include the effect of homogeneous soft modes, their relevance is easily underestimated in the theoretical analysis.

In 1D and 2D pattern-forming systems, most hydrodynamic modes are damped by the boundaries enclosing the system. For example, momentum and heat can usually diffuse freely through the boundaries and are stabilized by large external reservoirs. Obviously, this mechanism is ineffective in systems which are extended in all three spatial dimensions. On the other hand, some coupling to a reservoir will also be required in 3D in order to sustain non-equilibrium pattern formation. This could be through electromagnetic fields, some matrix embedding the active, pattern-forming medium, or some chemical reactant provided in excess. But the couplings to the reservoirs are highly specific in these cases and stabilize only a few hydrodynamic variables. The remaining fields do then lead to homogeneous soft modes. *As a result, several homogeneous soft modes should be considered as the rule in 3D, pattern-forming systems.*

For example, when studying the 3D structures formed by chemical waves in the Belousov-Zhabotinsky (BZ) reaction, the dynamics of the plain BZ reagent does also involve convective fluid motion. Since these hydrodynamic modes are usually considered to be a nuisance, they are suppressed by embedding the reagent in a gel [10]. But another homogeneous soft mode excited by the pattern, the temperature field (gradients of which are probably driving the convection) remains. Since temperature gradients have a strong influence on the dynamics of the pattern [11], a complete description of the 3D BZ reaction should explicitly involve this mode.

The work presented here is a case study of 3D pattern formation in the dielectric regime of electroconvection (EC) in nematic liquid crystals. The system was chosen because of its easy experimental accessibility. In particular, the electric nature of the instability allows to obtain patterns with several hundred periods extension in cells of a fingernail's size, evolving on the time scale of seconds. A closely related variant, the conduction regime of EC, which always leads to quasi 2D patterns, is currently one of the best understood experimental pattern-forming systems, on the phenomenological as well as on the quantitative level (see the reviews [12,13]). These advantages compensate the inconvenience of dealing with rather complicated (electro-)hydrodynamic equations.

Rather than trying to understand the complex pattern dynamics itself, this paper is mainly devoted to the development of consistent reduced descriptions of the dynamics. Section II sketches the experimental phenomenon and the hydrodynamics of dielectric EC, emphasizing its 3D nature. Approximations used for an analytic or semi-analytic description of dielectric EC are introduced in Section III, thereby discussing the linear stability problem. In Section IV the 3D amplitude formalism for dielectric EC is derived. Close to the threshold of EC and in a liquid-crystal slab of large but finite thickness,

the pattern dynamics becomes essentially 2D. The corresponding equations of motion are derived from the 3D formalism in Section V. In Section VI the stability of ideal periodic patterns is investigated and in Section VII a general scenario for the transition from the onset of dielectric EC to fully 3D pattern dynamics with increasing external stress is developed. Section VIII discusses possible experiments based on electric Nusselt number measurements and Section IX summarizes the results. Appendix A contains some analytic and numerical results for coupling coefficients, Appendix B compares two different methods for integrating multiple, homogeneous soft modes into the amplitude formalism in a general framework; one method is used in the main text.

II. SOME PHENOMENOLOGY OF ELECTROCONVECTION

Notice that below some points are oversimplified in order to ease intuition. For comprehensive reviews of EC see Refs. [12–14], for introductions into nemato-hydrodynamics Refs. [15,16].

A. Basic phenomena

In the typical experiment a nematic liquid crystal with negative dielectric anisotropy is sandwiched between a pair of transparent, parallel electrodes (separation $d \sim 20 - 50 \mu\text{m}$, area $\sim 1 \text{cm}^2$). By a special treatment of the electrode surfaces, the nematic director \vec{n} (the locally averaged molecular orientation; $|\vec{n}| = 1$) is forced to align parallel to the electrodes in some preferred direction which shall here be identified with the x -direction (z be normal to the electrodes, y normal to x and z). An ac voltage $E_0 \hat{z} d \cos \omega t$ is applied at the electrodes. In the *conduction regime* at frequencies below the *cut-off frequency* ω_c , the first instability to be observed as the voltage is increased is towards a pattern of convection rolls called Williams domains [17].

At higher frequencies a different kind of structure periodic along x is found. Compared to Williams domains it has shorter wavelength and decays faster after switching of the voltage (fast turnoff mode). At least two concurring mechanisms have been proposed for this high frequency mode: the *dielectric EC* [18], which depends essentially on the anisotropy of the nematic (its threshold diverges at the nematic-isotropic phase transition [19]), and the *isotropic mechanism* [20,21] where the liquid crystal's anisotropy is not essential for the convection mechanism itself but only for selecting a preferred modulation direction. It has a finite threshold at the nematic-isotropic phase transition as its characteristic signature [22]. The two linear modes have the same symmetry and do in principle mix, but generally the corresponding thresholds can be assumed to be sufficiently separated to

consider the mechanisms isolatedly. The isotropic mode is thought to be located mainly near the electrodes, while the dielectric mode is maximal at mid plane. Unfortunately, it is not always clear which mode is actually observed. At least in some cases the dielectric mode could be identified by the good match of the threshold curve with theoretical predictions (e.g. [23]). The isotropic mechanisms will not be considered here.

For voltages slightly higher than the threshold of dielectric EC, the formation of the *chevron* superstructure is observed: defects (dislocations) in the pattern of convection rolls accumulate along lines oriented in y direction, such that the topological charge of the defects alternates from line to line. Between the lines, the convection rolls are rotated and the nematic director is twisted, alternately clock- and counterclockwise [24]. The observation of chevron patterns in the conduction regime of EC with homeotropic director alignment [25,26] shows that this scenario is not restricted to a particular convection mechanism.

B. Hydrodynamic equations and material parameters

EC in both the conduction and the dielectric regime result from the interaction of electric field, space charges, mass flow, and the nematic director *via* the Carr-Helfrich [27] mechanism: Spatial modulations of the director orientation are amplified by an inhomogeneous mass flow generated by electric volume forces on space charges which accumulate due to inhomogeneous electric currents in the inhomogeneous director field. Thus Maxwell's equations¹ (in the quasi-static approximation² $\text{curl}\vec{E} = \text{curl}\vec{H} = 0$) and the balance equations for charge, momentum, mass (continuity equation), and the torque acting on \vec{n} have to be taken into account. They contain several material parameters: the conductivities $\sigma_{\parallel} \gtrsim \sigma_{\perp} = O(10^{-9} \dots 10^{-5} \Omega^{-1} \text{m}^{-1})$ for electric currents parallel (\parallel) and perpendicular (\perp) to \vec{n} respectively (they vary on a large range depending on purity and doping, while $\sigma_{\parallel}/\sigma_{\perp}$ changes only little), the dielectric constants³ $\epsilon_{\parallel}, \epsilon_{\perp} = O(\epsilon_0)$ (the quantities $\sigma_a := \sigma_{\parallel} - \sigma_{\perp} = O(\sigma_{\perp})$, $\epsilon_a := \epsilon_{\parallel} - \epsilon_{\perp} = O(\epsilon_{\perp})$ measure their anisotropies), the flexoelectric constants $e_1, e_3 = O(10^{-12} - 10^{-11} \text{C m}^{-1})$ ($e_+ := e_1 + e_2$, $e_- := e_1 - e_2$), the diffusion constants for (ionic) charge carriers $O(10^{-11} \text{m}^2 \text{s}^{-1}) =: D_{\rho}$, the mass density $\rho_m = O(10^3 \text{kg m}^{-3})$, the five independent viscosities $\alpha_1, \dots, \alpha_5 = O(0.1 \text{N m}^{-2} \text{s})$ ($\alpha_6 = \alpha_2 + \alpha_3 + \alpha_5$, $\gamma_1 = \alpha_3 - \alpha_2$, $\gamma_2 = \alpha_3 + \alpha_2$, $2\eta_1 = -\alpha_2 + \alpha_4 + \alpha_5$, $\eta_2 = \gamma_2 + \eta_1$), and the curvature elasticities of the direc-

tor field $k_{22} \lesssim k_{11} \lesssim k_{33} = O(10^{-11} \text{N})$. I also include the “dynamic flexoelectric effect”, which was predicted [28,29] on the basis of a systematic rederivation of nematohydrodynamics, but, to the authors knowledge, has not been detected, yet. It is characterized by a parameter ζ^E and leads to additional dissipative contributions in the charge, momentum, and torque balance equations.

C. Dimensional analysis

With the exception of the charge relaxation time $\tau_0 := \epsilon_{\perp}/\sigma_{\perp} = O(10^{-6} - 10^{-1} \text{s})$ the nematohydrodynamic equations (without external fields), being derived as a limit of large time and length scales (though typically valid down to molecular scales), do not set any time or length scale by themselves. Instead, one finds basically three types of diffusivities: for charge (D_{ρ}), director orientation [e.g. $D_{d,\text{stat}} = k_{33}/\gamma_1 = O(10^{-10} \text{m}^2 \text{s}^{-1})$ for static, $D_{d,\text{dyn}} = (k_{33}\eta_1)/(\gamma_1\eta_1 - \alpha_2^2) = O(10^{-9} \text{m}^2 \text{s}^{-1})$ for dynamic deformations; notice that (static) flexoelectric effects do not introduce a new diffusive scale since $e_{\pm}^2/\epsilon_0 \lesssim k_{33}$], and momentum [e.g. $D_p = (\gamma_1\eta_1 - \alpha_2^2)/(\gamma_1\rho_m) = O(10^{-5} \text{m}^2 \text{s}^{-1})$ along \vec{n}]. The overdamped limit $\rho_m \rightarrow 0$, $D_p \rightarrow \infty$ is generally a good approximation. Charge diffusion is not essential for the Carr-Helfrich mechanism and is typically screened out. Then orientational diffusion sets the only diffusive scale.

With an externally generated electric ac field $E_0 \hat{z} \cos \omega t$ two additional time scales are introduced: The period $2\pi\omega^{-1}$ and the “director time” $\tau_d = \gamma_1/(\epsilon_{\perp} E_0^2)$ [the more intuitive choice $\tau_d := \gamma_1/(\epsilon_a E_0^2)$ would suggest that $\epsilon_a = 0$ is singular for EC, which is, for the convective modes themselves, not the case].

In the conduction regime the charge densities oscillate with the frequency of the applied field, while the director orientation is mostly constant. This imposes a condition

$$\tau_d \gtrsim \omega^{-1} \gtrsim \tau_0 \quad (1)$$

on the three time scales. The finite sample thickness d determines the wavelength λ of the convection pattern and leads through a condition $d \sim \lambda \sim (D_{d,\text{stat}} \tau_d)^{1/2}$ to a voltage threshold $V_c^2 = d^2 E_c^2 \sim k_{33}/\epsilon_{\perp}$ for the onset of convection (see Ref. [13] for a good analytic formula). A lower limit for the sample thickness is given *via* relation (1) by $d^2 \gtrsim D_{d,\text{stat}} \tau_0$. At frequencies higher than the cutoff frequency $\omega_c \sim \tau_0^{-1}$ the conduction mechanism is also disabled or at least superseded by the dielectric mode.

¹In MKSA units.

²We will only allow for homogeneous magnetic fields.

³For convenience, the factor ϵ_0 is absorbed into ϵ_{\parallel} and ϵ_{\perp} .

In the dielectric regime director and fluid flow oscillate with ω , which leads to a condition

$$\tau_d \lesssim \omega^{-1}. \quad (2)$$

The charge distribution is at high enough frequencies ($\omega^{-1} \lesssim \tau_0$) mostly constant in time. This is not actually necessary for the dielectric mechanism to be effective [30], but typically dielectric EC is superseded by the conductive mode at lower ω . The threshold for the onset of EC is now given by a condition $\tau_d \sim \omega^{-1}$ (or $E_c^2 \epsilon_\perp / \gamma_1 \sim \omega$), i.e., the lowest E_0 compatible with relation (2). The wavelength λ of the critical mode can under some conditions be $\sim d$ [30], but for typical materials used it is $\lambda \sim (D_{d,\text{dyn}}/\omega)^{1/2}$, at least as long as this length is smaller than d and larger than the Debye screening length $(D_\rho \tau_0)^{1/2}$, i.e., $\omega \tau_0 < D_{d,\text{dyn}}/D_\rho = O(10^2)$, where charge diffusion becomes important.

Thus, the length scales given by the spatial period of the pattern λ and the sample thickness d are usually independent and easily separated ($\lambda \ll d$) in the dielectric regime, either by increasing d or by simultaneously increasing ω and the conductivities, while leaving the secondary control parameter $\omega \tau_0$ constant. Since strong doping may affect the nematic material parameters and the nematodynamics at high frequencies is not fully understood, the program carried out below is best seen as the *limit of thick cells*. The theory should accurately describe typical experiments in cells with $d \gtrsim 10 \lambda$. To observe fully three dimensional patterns, thicker cells might be required (see also Section VII).

III. APPROXIMATION METHODS AND LINEAR THEORY

A. 2D vs. 3D amplitude formalism

Below we will develop the amplitude formalism for the pattern dynamics in the dielectric regime, i.e., obtain the laws of motion of amplitude and phase of the spatial modulations as described by the complex pattern amplitudes $A'(x, y, t)$ or $A(x, y, z, t)$, respectively.

The basic state in the experimental cell is anisotropic and inversion symmetric and the primary bifurcation is supercritical (forward) towards a steady-state pattern with a single critical wave vector. Hence, the most elementary description of the pattern dynamics is given by the time-dependent Ginzburg-Landau equation in 2D,

$$\tau \partial_t A' = (\epsilon' + \xi_x^2 \partial_x^2 + \xi_y^2 \partial_y^2 - g' |A'|^2) A', \quad (3)$$

important physical properties of which are reviewed in Refs. [31,32]. The real, positive coefficients τ , ξ_x , ξ_y , and g' have magnitudes corresponding to natural scales of the system (e.g. the pattern wavelength for ξ_x , ξ_y) and can be calculated from the underlying hydrodynamic equations. The small, dimensionless parameter ϵ' measures

the distance from the threshold of pattern formation in the control-parameter space of the underlying system.

It will be shown in Sec. V that, as a direct consequence of the separation of length scales in the dielectric regime, the range of validity of Eq. (3) is highly restricted. Already for values of ϵ' of the order λ^4/d^4 corrections to Eq. (3) must be taken into account. For $\epsilon' \sim \lambda^2/d^2$ the 2D description breaks down completely. But the convective dynamics can then still be described in terms of the 3D modulations of the complex pattern amplitude $A(x, y, z, t)$ (defined by Eq. (4) below), which is coupled nonlinearly to several homogeneous soft modes. It is therefore natural to derive first the 3D amplitude dynamics which can then be reduced further to a 2D description in a subsequent step.

Julien, Knobloch, and Tobias [2,3] were the first to implement the idea of deriving a reduced description for the z -dependence of the amplitude of patterns with $\lambda/d \ll 1$ as an intermediate step in the theory, and also the first to observe that this method significantly eases the restriction of the control parameter to values close to threshold. Their calculation does, however, not involve in-plane modulations of the pattern and the resulting excitation of homogeneous soft modes. Several results concerning the 3D description of dielectric EC and its reduction to 2D are derived in an unpublished work by Lindner [33], which is quoted here whenever necessary.

B. Linear stability in 3D

The starting point for setting up the 3D amplitude equations is to calculate the linear threshold E_c , critical wave number q_c and critical eigenvector (i.e., the $2\pi/\omega$ -periodic time dependence of the hydrodynamic fields at threshold) ignoring any spatial variations along z . Several linear stability calculations of this type have been carried out [18,30,34,13].

In experiments, the critical wave vector is always found to be parallel to the orientation of the nematic director in the basic state (the x direction). The linear problem is thus effectively one-dimensional, with trivial, sinusoidal variations along the remaining x direction, and is much easier to solve than the 2D problem including variations and boundary conditions along z . This technical advantage of the 3D approach, which is of course not restricted to EC, remains effective also in the subsequent calculations of the coupling coefficients in the 3D amplitude equation.

For analytic as well as numerical calculations it is convenient to use a truncated Fourier expansion of the time dependences of the hydrodynamic fields, assuming them to be $2\pi/\omega$ periodic. In the simplest cases truncated at lowest order (i.e., including constant and $\sin/\cos \omega t$ contributions) [13,33] or including the $\sin/\cos 2\omega t$ modulation of the induced electric potential in order to better model the interplay between electric charges and

fields. With these truncations, the stability problem for sinusoidal excitation can be solved explicitly (see Appendix A). Notice, however, that this “lowest order” or, respectively, “second lowest order Fourier approximation” involves some arbitrariness in the choice of variables and does not correspond to any physical limit. Numerical convergence (5% accuracy) requires inclusion of at least the third harmonic. The actual time dependence of, e.g., the director field, depends on ω and is non-trivial even as $\omega \rightarrow \infty$ [18].

Some results presented here rely on the first or second lowest order Fourier expansion of the induced electric potential Φ , the nematic director expressed by n_z and φ such that $\vec{n} = n_z \hat{z} + (1 - n_z^2)^{1/2} \hat{c}$, $\hat{c} := (\cos \varphi, \sin \varphi, 0)$, the velocity field \vec{v} , and the pressure P . The other hydrodynamic fields are treated implicitly. For the representation of the dielectric mode itself, \vec{v} is expressed in the divergence-free form $\vec{v} = (-\partial_y, \partial_x, 0)g + (\partial_x \partial_z, \partial_y \partial_z, -\partial_x^2 - \partial_y^2)f$ and the pressure is eliminated.

As a natural consequence of $\tau_d \sim \omega^{-1}$, the relative phases of electric, director and velocity fields in the linear eigenvector are shifted by angles $O(1)$. Remarkably, the phase shift between the lowest Fourier mode of director oscillations and external field is $\pi/4$, for the first [33] and second-lowest-order Fourier approximation (see Appendix A) exactly and only slightly perturbed ($< 1\%$ for $\omega\tau_0 > 2$) when higher Fourier modes are included. No simple physical explanation for this result should be expected, since it holds only at the critical (most unstable) wavenumber. Experimental observations [35] seem to agree with a value $\pi/4$ for the phase shift even better than the comparison with Galerkin calculations including z -dependence [36], which had been carried out as a test of the dielectric model of EC.

We define the pattern amplitude A such that the amplitude $n_{z,c}$ of the $\cos \omega t$ Fourier component of the director tilt oscillations (which is in phase with the applied voltage) has a spatial dependence

$$n_{z,c} = A(x, y, z, t) \exp(iq_c x) + c.c. \quad (4)$$

Assuming as usual ϵ , ∂_x , ∂_y , ∂_z to be small and discarding contributions beyond the lowest nontrivial order, the linear part of the 3D amplitude equation assumes the form

$$\tau \partial_t A = (\epsilon + \xi_x^2 \partial_x^2 + \xi_y^2 \partial_y^2 + \xi_z^2 \partial_z^2) A. \quad (5)$$

As conventional, $\epsilon := (E_0^2 - E_c^2)/E_c^2$. The coherence lengths ξ_x , ξ_y , ξ_z turn out to be $\sim \lambda$ and the relaxation time τ is of the order of the charge relaxation time τ_0 [30] (s. Appendix A).

The horizontal boundary conditions for A are simply

$$A = 0 \quad \text{at} \quad z = \pm d/2. \quad (6)$$

Contributions from derivatives of A and nonlinear contributions to the boundary conditions are of higher order and can be discarded. In particular, as is well known, the

distinction between free and no-slip boundary conditions for the velocity field plays no role at this point. With the realistic no-slip boundary conditions for the velocities, the relative magnitude of the hydrodynamic fields in the 2D linear eigenvector (including x and z variations) locally deviates from the 1D eigenvector (only x variation) only in a boundary layer of thickness $\sim \lambda$, an example of which is shown in Fig. 1. This boundary layer might provide a problem for numerical approaches directly using 2D eigenvectors in thick cells with no-slip boundaries, notably when Galerkin approximations are used.

C. Linear stability in a cell of finite thickness

Assuming as usual the lateral (x, y) extensions of the cell to be large compared to its thickness d , the trivial solution $A \equiv 0$ of Eq. (5) with boundary conditions (6) becomes unstable at $\epsilon = \epsilon_d := (\pi \xi_z / d)^2$ [i.e., $\epsilon' = \epsilon - \epsilon_d$ in Eq. (3)] with a critical mode $A \sim \cos(\pi z / d)$. The small threshold shift $E_c \rightarrow (1 + \epsilon_d / 2) E_c$ due to the z -variation is rather uninteresting by itself (there is also a shift $\sim \lambda^2 / d^2$ in q_c by a discarded contribution to Eq. (5) of the form $i \partial_x \partial_z^2 A$), but the effect provides, for example, a simple interpretation of the small gap ($\Delta E_0 = 3\epsilon_d E_c / 2$) between the critical mode and the lowest z -antisymmetric mode (i.e. $A \sim \sin(2\pi z / d)$) reported in [37].

D. Flexoelectric effects

A short remark about flexoelectric effects, which are generally difficult to isolate experimentally, is in place at this point. The high symmetry of the linear problem in 3D does not allow flexoelectric effects: E_c , q_c , τ , and ξ_x are independent of the flexoelectric coefficients. Most of the remaining linear and nonlinear coefficients contain flexoelectric contributions. With our choice of variables these contributions are, except for some dynamic-flexoelectric terms, all indirect: flexoelectric effects excite additional, “slaved” contributions in the subspace orthogonal to the critical eigenvector, which, again by flexoelectric effects, feed back into the dynamics of the amplitude of the eigenvector. In contrast, the contributions not depending on flexoelectric coefficients are, except for ξ_x , all direct: no excitation of slaved degrees of freedom is involved. Therefore *flexoelectric effects are separated in a natural way* from the standard dynamics. This might provide methods for measuring the flexoelectric coefficients in a way not sensitive to parasitic boundary effects. Previous calculations involving flexoelectric effects [34,38,39] were restricted to the conventional, “static” flexoelectric contributions and concentrated on the determination of critical mode and voltage.

IV. THE 3D AMPLITUDE EQUATIONS

A. Method

Before discussing the homogeneous soft modes relevant for dielectric EC, some comments on methodology are required.

Multiple homogeneous soft modes excited by a patterning mode have, to my knowledge, first been introduced by Plaut and Pesch [40]. But their description requires the soft-mode amplitudes to be constant along all but one spatial direction. This limitation seems to be partly due to the procedure by which the equations were derived. There are two popular philosophies for this procedure (see below and Appendix B), which shall here be labeled as “order parameter” method and “center manifold” method. The two methods usually (for at most one homogeneous soft mode) differ only in the way in which the problem is formulated and solved, but lead to the same results. The association of existing general prescriptions for deriving amplitude equations with the former (e.g. [41–44,32]) and the latter philosophy (e.g. [45,46], the Chapman-Enskog approach [47,48] for the derivation of hydrodynamics from statistical mechanics is also of this type, see Refs. [49,50]) is therefore not always conclusive (see also [31,51,52]). When using the “order parameter” method to obtain reduced equations, each spatial Fourier mode of the physical state is projected onto the (adjoint) slowly decaying linear eigenmodes of the basic state *with the corresponding wave vector*. Using the “center manifold” method, the projection is always onto the (adjoint) eigenvectors for (typically neutrally stable) *homogeneous perturbations*. When there are multiple slow modes at a single wave vector (usually $\vec{q} = 0$), the resulting reduced equations differ, as is shown in Appendix B. Plaut and Pesch [40] seem to be using the “order parameter” method, which leads to problems in more than one spatial dimension. Here, the “center manifold” method is used to derive the nonlinear extensions of the amplitude equation (5) including homogeneous soft modes.

B. Derivation of the soft mode equations

Some particularities of the problem under consideration have to be taken into account: The quasi-static approximation of electrodynamics $\text{curl } \vec{E} = 0 = \text{curl } \vec{B}$ and the approximation of an incompressible fluid $\nabla \vec{v} = 0$ both lead to additional homogeneous “soft modes”: Since no time derivatives of electric potential (electric field) or pressure occur in the basic equations as they are used here, all their temporal Fourier modes are in the kernel of the linear operator $L(0, 0)$ (s. Appendix B). When the viscid limit $\rho_m \rightarrow 0$ becomes effective, the same applies for the oscillating part of the velocity field. This is the case when spatial variations occur on scales smaller than $(\omega D_p)^{1/2} = (D_p/D_{\text{dyn}})^{1/2} \lambda = O(10^{5/2})\lambda$. Formally we

shall assume length scales to be larger than this. But, since, at least in this case, velocity and pressure oscillations do not feed back into the remaining dynamics at lowest order in the derivatives, i.e., there are no contributions $O(\rho_m^{-1})$, the description should be good also on smaller scales.

To simplify the problem further, the equations for the soft modes are here calculated only in the lowest order Fourier approximation. The “slaved” modes being eliminated are then the slowly varying average director tilt n_z , which is stabilized by the applied electric field through the dielectric anisotropy ϵ_a (assumed to be negative hereafter), and oscillations of the director, which are viscously damped. Finally, in anticipation of corresponding boundary conditions, only small deviations from the basic state $\vec{v}, \varphi, n_z, \Phi = 0$ shall be considered for now.

In order to obtain a consistent truncation of the soft-mode equations, recall that the only non-diffusive scale in the hydrodynamic equations is the charge relaxation time τ_0 . Assume $\omega\tau_0$ to be fixed. This also determines $E_c \sim \omega^{1/2}$ for given τ_0 and we will assume $E_0 \approx E_c$. The elimination the fast modes (n_z and oscillations of \vec{n}) becomes more efficient when ω and E_0 increase or, respectively, τ_0 decreases. Then, in the limit of small τ_0 (or large σ_{\parallel} , with fixed $\sigma_{\parallel}/\sigma_{\perp}$), the time scale τ_0 drops out of the equations. A purely diffusive scaling for the derivatives ($\partial_x^2 \sim \partial_y^2 \sim \partial_z^2 \sim \partial_t$) is retained, without making any *a priori* assumptions about the actual scaling laws of typical lengths and times, which may be different. This approximation breaks down when length scales become shorter than $(D_{d,\text{stat}}\tau_0)^{1/2}$ or $(D_{d,\text{stat}}/\omega)^{1/2}$.

It turns out that with these approximations the only *relevant* modes in the fast subspace (i.e. R in Appendix B 3) are n_z and its temporal modulations as given by

$$\begin{aligned}
 n_z(x, y, z, t) = & \\
 & 2\partial_z \frac{(k_{22} - k_{11}) \partial_y n_y + \alpha_3 v_x}{E_0^2 \epsilon_a} \\
 & + 2\partial_x \frac{\epsilon_a E_0 \Phi_r - (e_+ - 2\gamma_1 \zeta^E) \partial_z \Phi_0 + \alpha_2 v_z}{E_0^2 \epsilon_a} \quad (7) \\
 & + \frac{2b(\epsilon_a \partial_x \Phi_0 - e_- \partial_y n_y)}{E_0^3 \epsilon_a^2} \times \\
 & \quad (E_0^2 \epsilon_a \cos(\omega t) - 4\gamma_1 \omega \sin(\omega t)).
 \end{aligned}$$

The electric potential has been decomposed as $\Phi = \Phi_0 + 2\Phi_r \cos \omega t - 2\Phi_i \sin \omega t$. The parameter $b := E_0^4 \epsilon_a^2 / (3 E_0^4 \epsilon_a^2 + 16 \gamma_1^2 \omega^2)$ measures the strength of the excitation of the oscillatory part of n_z . It is numerically small [in the standard material MBBA (*p*-methoxybenzilidene-*p'*-*n*-butylaniline) $b \approx 0.01$]. The resulting description for the soft mode dynamics is given by the Eq. (40) on page 15 (for the terms containing A , see Section IV F below).

C. Comments on the soft mode equations

Most of the terms in Eq. (40) reproduce linearized nematic hydrodynamics. Equations (40a-40c) derive from the charge balance equation [Eqs. (40b,40c) have been multiplied with E_0], Eq. (40d) from the angular momentum balance on \vec{n} , Eqs. (40e-40g) from the Navier-Stokes equation and Eq. (40h) is the unchanged continuity equation. In Eq. (40d) a term $\chi_a H_y^2 \varphi$ has been included, which describes the action of a magnetic field in y direction. It will be used in Section V. The contributions resulting from the elimination of fast modes are underlined.

Remarkably, the equations are mostly independent of the strength of the external field (a factor E_0 can be absorbed into the definitions of Φ_r and Φ_i), although it is the cause for the excitations of the slaved modes. As an example, consider the mechanism for the reduction of viscosity by the term $\alpha_2 \partial_x^2 v_z$ in Eq. (40g) (recall $\alpha_2 < 0$): Shear forces $\sim \alpha_2 \partial_x v_z$ excite n_z . This leads to polarization charges $\sim \partial_x E_0 \epsilon_a n_z$. The electric field $\sim E_0$ acting on these charges generates bulk forces on the fluid. On the other hand, the excitation of n_z is damped by electric forces $\sim \epsilon_a E_0^2$ and the factor E_0^2 cancels out.

The soft mode equations reflect the non-equilibrium character of the basic state. For example, if Onsager's relations would hold, the coefficients of $\partial_x \partial_z v_x$ in Eq. (40g) and of $\partial_x \partial_z v_z$ in Eq. (40e) would be the same. At low ω the basic state is even unstable. The mechanism corresponds to EC in the conduction regime. Ignoring flexoelectric effects, the cutoff frequency ω_c above which the basic state stabilizes is given by

$$\omega_c^2 = \frac{\sigma_{\parallel} (\alpha_2 \epsilon_{\perp} \sigma_{\parallel} - \alpha_2 \epsilon_{\parallel} \sigma_{\perp} - \epsilon_a \eta_1 \sigma_{\perp})}{\epsilon_a \epsilon_{\parallel} \epsilon_{\perp} \eta_1}, \quad (8)$$

which reproduces the result of direct stability calculations using (effectively) the same Fourier truncation [18]. Only the threshold field for the Williams domains is too small to be resolved by Eq. (40).

D. Nonlinear extensions

Of course, constant values can always be added to any of the soft modes by a Galilei transformation, a rotation, or a gauge transformation. The problem of adding nonlinear contributions (e.g. advection terms) to Eqs. (40) such that they become formally invariant under these transformation is easily solved. The solution is not unique, but it can be seen by inspection that the precise form of the nonlinearities does not matter under the following conditions:

1. Dynamics is such that, in fact, diffusive scaling holds. In particular this implies that, if $L \gg \lambda$ is the typical length scale (i.e. $\partial_x, \partial_y, \partial_z \sim L^{-1}$), the variations of \vec{v} , Φ_r , Φ_i , φ/L , and Φ_0/L over L scale in the same manner as $L \rightarrow \infty$.

2. Variations in φ over L are much smaller than one. It is not necessary to specify the scaling relation of φ and L . When L is determined through the bulk dynamics, φ may actually vary by $O(1)$ over the sample.

It should be noticed that, although the second condition is satisfied for many problems of pattern dynamics, it is too strong for disclinations (line defects) in the director field at any distance R from the core of the disclination: On the typical length scale $L = R$ variations of φ are $O(1)$. Then, for example, nontrivial nonlinear contributions from the velocity field $\vec{v} \sim L^{-1}$, like a term of the form $(\partial_x v_z)(\partial_y \varphi)$ in Eq. (40g), might have to be included.

For the part describing the curvature elasticity in Eq. (40d), the fully nonlinear corrections in φ have been calculated by extending the ‘‘center manifold’’ method to nonlinear contributions and requiring rotation invariance. The result has the same form as close to equilibrium:

$$\begin{aligned} \gamma_1 \partial_t \varphi &= k_{33} \hat{c}_{\perp} \cdot (\partial_x^2 + \partial_y^2) \hat{c} \\ &+ (k'_{11} - k_{33}) (\hat{c}_{\perp} \cdot \nabla) (\nabla \cdot \hat{c}) + k_{22} \hat{c}_{\perp} \cdot \partial_z^2 \hat{c} + \dots \end{aligned} \quad (9)$$

$[\hat{c}_{\perp} := (-\sin \varphi, \cos \varphi, 0)]$, however, with $k'_{11} := k_{11} + 2b e_-^2 / \epsilon_a$. Although an additional term proportional to $(\nabla \cdot \hat{c}_{\perp})(\nabla \cdot \hat{c})$ would be thinkable, it does not occur in the present approximation. For a rotationally invariant description of the dynamics of the convection pattern, it is useful to go over to a representation in terms of $\hat{A}(\vec{r}) = A(\vec{r}) \exp(iq_c x)$ as in Ref. [53].

E. Stability of the twist mode with respect to x modulations

Another point to notice is that below the threshold of dielectric EC (i.e. with $A = 0$) the system can, in our approximation, never destabilize in such a way that φ is excited but $\partial_y \varphi = 0$, even when allowing for flexoelectric effects and arbitrary z dependencies. Without y modulations, the in-plane director couples only to v_x , and this interaction is not affected by the elimination of the fast modes and hence relaxational. This is remarkable because such modulation instabilities of φ below the EC threshold are apparently *observed in experiments* [19,54] (the ‘‘inertial mode’’ [55] which was proposed as an explanation has the wrong symmetry). A far-fetched but possible explanation would be that the modulations in φ are generated through a mechanism which is similar to the one that generates the chevron superstructure in the dielectric regime, however, invoked by the convection rolls of ‘‘isotropic’’ EC (see Section II A). The isotropic mechanism is expected to become active in the respective experimental situations but does itself not involve excitations of φ . The convection rolls might themselves be

smaller than the optical resolution and therefore remain unobserved. Then the onset of φ modulation would *appear* to be the threshold of a primary instability of the homogeneous basic state, although the actual primary (“isotropic”) threshold is at slightly lower voltages.

F. Interaction with the pattern

The equation of motion for the pattern amplitude itself is given by

$$\begin{aligned} \tau(\partial_t + \vec{v} \cdot \nabla + iv_x q_c)A = & \left[\kappa_x \nabla_x v_x + \kappa_z \nabla_z v_z \right. \\ & + \xi_x^2 \partial_x^2 + \xi_y^2 (\partial_y^2 - 2iq_c \varphi \partial_y - q_c^2 \varphi^2) + \xi_z^2 \partial_z^2 \\ & \left. + i\alpha_x \nabla_x \Phi_0 + i\beta_y \nabla_y \varphi - \frac{4\nabla_z \Phi_r}{E_c} + \varepsilon - g|A|^2 \right] A. \quad (10) \end{aligned}$$

All coefficients are real. The differential operators ∇_x , ∇_y , ∇_z are used to indicate that only the immediately following expression should be differentiated, not A . With the exceptions of $v_x \partial_x A$ and $\nabla_x v_x A$, which are included for symmetry, only terms up to lowest nontrivial order have been included, assuming time, all lengths and all fields to scale independently. The l.h.s. is given by Galilean invariance, the form of the expression following ξ_y^2 from rotation invariance [56]. The term involving $\nabla_z \Phi_r$ represents simply an additional contribution to the electric driving field. Symmetry would also allow a term $\kappa_y \nabla_y v_y A$, but the hydrodynamic equations do not generate it.

When $\beta_y = -\xi_y^2 q_c$ it is possible to absorb the corresponding term into the parenthesis after ξ_y^2 and to rewrite the complete expression in the “potential” form $\xi_y^2 (\partial_y - iq_c \varphi) (\partial_y - iq_c \varphi) A$. In this case the phase of the pattern does not drift in a weakly deformed φ field. In fact, β_y is close to this value (see [33], Appendix A), which is largely due to the conservation of charge and momentum and the flux-divergence form of the resulting expressions.

The Landau coefficient g is of order unity in our normalization [33]. As in the conduction regime [40], it is dominated by “geometric” effects, i.e., inhibition of the Carr-Helfrich mechanism for large n_z : besides flexoelectric effects, about 99% of g come from contributions quadratic or cubic in n_z . This indicates that a breakdown of the weakly nonlinear expansion should be expected for $A \sim n_z = O(1)$.

The nonlinear excitation of the soft modes by the convection pattern is less intuitive than their feedback onto the rolls discussed above. The principle of truncation for the contributions of A in Eq. (40) is again to keep only terms of lowest nontrivial order, however, allowing for phase gradients of A without gradients of the modulus. As the relative scaling of φ *vs.* length scales is left undetermined at this stage (see Section IV D), the nonlinear

term $-A^* iq_c \varphi A$, which is given by rotation symmetry, must always come along with $A^* \partial_y A$.

Since Eq. (40a) must have flux-divergence form, the largest contributions from A are $O(\nabla^2 A^2)$, which is too small to be relevant. The coefficients I_r and I_i in Eqs. (40b,40c) have the dimensions of a current density and measure the strength of an alternating current $\vec{j}_{|A|^2} = 2|A|^2 (I_r \cos \omega t - I_i \sin \omega t)$ generated by the convection pattern. Important contributions to the coefficients I_r, \dots, I_{iz} come from charge advection.

The strongest contributions to Γ in Eq. (40d) are simple potential effects. In MBBA, the most important one describes a relaxation of the bend of the director modulations by twist and is given by $4(k_{22} - k_{33})$ (see [33,40] and Appendix A), which is generally negative. The second most important contribution comes from the dielectric torques from applied and induced field on the director. In MBBA this contribution to Γ is positive and in materials with large negative ϵ_a (e.g. $\lesssim -\epsilon_\perp$) it could compensate the elastic one and reverse the sign of Γ . Notice also that Γ is particularly sensitive to flexoelectric effects (s. Table I). A negative value of Γ is required for the occurrence of abnormal rolls (see Sec. VI A) and chevron patterns.

The terms associated with S_x and S_z in Eqs. (40e,40g) represent internal stresses of the convection pattern. As for the coupling of A to \vec{v} in Eq. (10), a corresponding term for the y direction or a term of the form $S_{yx} \partial_y \text{Im}\{A^* \partial_x A\}$ do not enter Eq. (40f), although they are allowed by symmetry. $S_{xx}, S_{yy}, \dots, S_{zx}$ can be interpreted as surface tensions of the planes of equal phase of the convection pattern.

The high number of soft modes and the rich, non-potential coupling almost certainly lead to spatio-temporally chaotic states already at onset, provided the spatial extensions of the sample are large enough.

V. EFFECTIVELY 2D PATTERN DYNAMICS NEAR THRESHOLD

Currently more interesting than the fully 3D chaotic state are, from the experimental point of view, the quasi 2D pattern dynamics in a restricted geometry near threshold [$e' \lesssim (\lambda/d)^2$]. The dynamics is here derived for a slight generalization of the usual setup: A magnetic field H_y might be applied along the y direction (i.e. in-plane, normal to the rubbing direction). With H_y slightly below the twist Freédericksz field $\chi_a H_F^2 = k_{22} (\pi/d)^2$, the amplitude of the twist mode, which is known to be important for the pattern dynamics in any case, becomes a slow variable and must be included explicitly in the 2D formalism. The conventional setup is described by $H_y = 0$.

A. Derivation of the 2D description

The appropriate boundary conditions for the soft modes at the enclosing electrodes are

$$\Phi_0, \Phi_r, \Phi_i, \varphi, \vec{v} = 0 \quad \text{at} \quad z = \pm d/2. \quad (11)$$

Thus, all components of the electric potential and the velocity field are damped by the boundaries.

Again the ‘‘center manifold’’ method is used (s. Appendix B), now to reduce the 3D equations to 2D. The dynamically active part S of the state vector U is now given by the sum of

$$A(x, y, z) = A'(x, y) \cos(\pi z/d), \quad (12)$$

$$\varphi(x, y, z) = \varphi'(x, y) \cos(\pi z/d), \quad (13)$$

$$P(x, y, z) = P'(x, y), \quad (14)$$

with the amplitudes of the active modes A' , φ' , and P' .

To be specific, associate A with the complex conjugate of Eq. (10) and Φ_0 , Φ_r , Φ_i , φ , v_x , v_y , v_z , and P with successive equations in the system (40), and define the scalar product $\langle \cdot | \cdot \rangle$ as usual as the equally weighted sum over z integrals over products of the two components. The projector onto the slow dynamics is constructed from the bi-orthonormalized linear functionals $(2/d) \int_{-d/2}^{d/2} \cos(\pi z/d) A dz$, $(2/d) \int_{-d/2}^{d/2} \cos(\pi z/d) \varphi dz$, and $(1/d) \int_{-d/2}^{d/2} P dz$.

We proceed with a calculation of the excitations in the fast subspace R by a term-by-term solution of Eq. (B12). The truncation is chosen such that the distinguished limit

$$\begin{aligned} P', H_F^2 - H_y^2, \partial_t \sim \varepsilon', \\ \varphi', A', \partial_x, \partial_y \sim \varepsilon'^{1/2}, \\ \varepsilon' = O(\lambda/d)^4, \quad \text{and} \quad d \rightarrow \infty \end{aligned} \quad (15)$$

is correctly described.

At linear order in the amplitudes and to linear order in ∂_x, ∂_y , the slaved part of the state vector contains only the contributions

$$v_x^{(1)} = -\frac{1}{\eta_2} \left(\frac{d^2}{8} - \frac{z^2}{2} \right) \partial_x P', \quad (16)$$

$$v_y^{(1)} = -\frac{2}{\alpha_4} \left(\frac{d^2}{8} - \frac{z^2}{2} \right) \partial_y P'. \quad (17)$$

At order $O(|A'|^2)$ and without any x or y modulations there are excitations of the electric field

$$\Phi_r^{(2)} + i\Phi_i^{(2)} = \frac{I_r + iI_i}{\sigma_\perp + i\omega\epsilon_\perp} \int_{-d/2}^z |A(z')|^2 - \langle |A|^2 \rangle_z dz', \quad (18)$$

and a contribution to the pressure field, orthogonal to the active pressure mode,

$$P^{(2)} = -(S_z - 2S_E) \cdot (|A|^2 - \langle |A|^2 \rangle_z), \quad (19)$$

where $\langle |A|^2 \rangle_z = |A'|^2/2$ is the average of $|A|^2$ over z and

$$S_E := \frac{E_0 \epsilon_\perp (\omega \epsilon_\perp I_i + \sigma_\perp I_r)}{\omega^2 \epsilon_\perp^2 + \sigma_\perp^2}. \quad (20)$$

By gradients of $\Phi_r^{(2)}$, $\Phi_i^{(2)}$, $P^{(2)}$, and by direct contributions at order $O(\partial_x |A'|^2, \partial_y |A'|^2)$ the mean flow

$$v_x^{(2)} = \left[S_x \left(\frac{d^2}{16} - \frac{z^2}{4} \right) + (S_E + S_x - S_z) \frac{d^2}{4\pi^2} \cos^2\left(\frac{\pi z}{d}\right) \right] \frac{\partial_x |A'|^2}{\eta_2}, \quad (21)$$

$$v_y^{(2)} = (S_E - S_z) \frac{d^2}{4\pi^2} \cos^2\left(\frac{\pi z}{d}\right) \frac{2\partial_y |A'|^2}{\alpha_4}. \quad (22)$$

is excited (there is no distinction between ‘‘singular’’ and ‘‘non-singular’’ mean flow in this approach). Excitations of Φ_0 are of the order $O(\varepsilon')$ and do, as all other remaining corrections, not contribute at leading order.

Projection of the dynamics with the full state vector $U = S + R$ onto the slow space yields the equations of motion for the pattern amplitude

$$\tau \partial_t A' = \left[\xi_x^2 \partial_x^2 + \xi_y^2 \left(\partial_y^2 - \frac{16iq_c}{3\pi} \varphi' \partial_y - \frac{3q_c^2}{4} \varphi'^2 \right) \right] A' \quad (23a)$$

$$+ i \frac{8}{3\pi} \beta_y \nabla_y \varphi' + \epsilon' - \left(\frac{3}{4} g + \frac{S_E}{\epsilon_\perp E_0^2} \right) |A'|^2 \quad (23b)$$

$$- \frac{id^2 q_c \tau}{48\pi^2} \frac{9S_E + (15 + 2\pi^2)S_x - 9S_z}{\eta_2} \nabla_x |A'|^2 \quad (23c)$$

$$+ \frac{id^2 q_c \tau}{12\pi^2} \frac{3 + \pi^2}{\eta_2} \nabla_x P' \Big] A' \quad (23d)$$

and the twist mode,

$$\gamma_1 \partial_t \varphi' = (k_{33} \partial_x^2 + k'_{11} \partial_y^2 - \chi_a (H_F^2 - H_y^2)) \varphi' \quad (24a)$$

$$+ \frac{q_c \Gamma}{2} \text{Im} \left\{ A'^* \left[\frac{8}{3\pi} \partial_y - \frac{3iq_c}{4} \varphi' \right] A' \right\} \quad (24b)$$

$$+ \frac{4d^2}{\pi^3} \left[\frac{\alpha_3}{\eta_2} + \frac{2\alpha_2}{\alpha_4} \right] \partial_x \partial_y P' \quad (24c)$$

$$- \frac{2d^2}{3\pi^3} \left[\frac{2\alpha_2 (S_E - S_z)}{\alpha_4} + \frac{\alpha_3 (S_E + 4S_x - S_z)}{\eta_2} \right] \partial_x \partial_y |A'|^2, \quad (24d)$$

and the pressure Poisson equation [1]

$$0 = -\frac{d^2}{12} \left[\frac{1}{\eta_2} \partial_x^2 + \frac{2}{\alpha_4} \partial_y^2 \right] P' \quad (25a)$$

$$+ \frac{d^2}{8\pi^2} \frac{S_E + (1 + \pi^2/3)S_x - S_z}{\eta_2} \partial_x^2 |A'|^2 \quad (25b)$$

$$+ \frac{d^2}{4\pi^2} \frac{S_E - S_z}{\alpha_4} \partial_y^2 |A'|^2. \quad (25c)$$

B. Remarks on the 2D amplitude equations

By the explicit representation of the coupling coefficients in Eqs. (23-25), the increasing importance of the mean flow contributions in lines (23c, 23d, 24c, 24d) as the separation d of the damping boundaries increases becomes obvious. On the other hand, for small enough d , i.e. $\varepsilon' \ll (\lambda/d)^4$, mean flow is negligible. With some rescaling (indicated by a caret $\check{}$) dynamics are then described by the system

$$\check{\tau} \partial_{\check{t}} \check{A} = \left[1 + \partial_{\check{x}}^2 + \partial_{\check{y}}^2 - 2i c_1 \check{\varphi} \partial_{\check{y}} - c_2 \check{\varphi}^2 - |\check{A}|^2 + i \check{\beta}_{\check{y}} \check{\varphi}_{,\check{y}} \right] \check{A}, \quad (26a)$$

$$\partial_{\check{t}} \check{\varphi} = \partial_{\check{y}}^2 \check{\varphi} + \check{K}_3 \partial_{\check{x}}^2 \check{\varphi} - \check{H}^2 \check{\varphi} + 2\check{\Gamma} \text{Im} \{ \check{A}^* (\partial_{\check{y}} - i \check{\varphi}) \check{A} \}. \quad (26b)$$

This is the “normal form” for the dynamics of a pattern coupled to a soft mode with symmetry under the reflections $[\check{x} \rightarrow -\check{x}, \check{\varphi} \rightarrow -\check{\varphi}, \check{A} \rightarrow \check{A}^*]$ and $[\check{y} \rightarrow -\check{y}, \check{\varphi} \rightarrow -\check{\varphi}]$ or $[\check{y} \rightarrow -\check{y}, \check{\varphi} \rightarrow -\check{\varphi}, \check{A} \rightarrow -\check{A}]$. In the present case $c_1 = c_2 = \frac{4}{3} \left(\frac{8}{3\pi} \right)^2 \approx 0.96$ are fixed by geometric constraints [33]. These values are quite close to the case with an underlying rotation symmetry $c_1 = c_2 = 1$ [56], which turns out to be somewhat singular in its dynamical properties [57,58].

With $H_y^2 = 0$ in line (24a), φ' is damped out and becomes one of many higher order corrections. Equations (23, 25) with $\varphi = 0$ are then sufficient, and with $\varepsilon' \ll (\lambda/d)^4$ the simple Ginzburg-Landau Equation (3) with

$$g' = \frac{3}{4}g + \frac{S_E}{\varepsilon_{\perp} E_0^2} \quad (27)$$

(the second contribution is numerically small, see Table I) is retained.

When modulations of $|A|^2$ along x are strong, like in the chevron pattern, it is instructive to redefine the pressure $P' \rightarrow P' - \text{const.} \times |A|^2$ such that its excitation by $\partial_x^2 |A|^2$ in line (25b) is canceled. It turns out that the remaining excitation of P' by $\partial_y^2 |A|^2$ is proportional to S_x . The substitute for line (23c) incorporating the correction in P' does then have the form

$$-\frac{id^2 q_c \tau (\pi^2 - 6)}{16\pi^4} \frac{S_E + S_x - S_z}{\eta_2} \nabla_x |A|^2$$

and accounts for a mean flow with a nontrivial flow profile with zero z average.

C. Pressure vs. singular mean flow

As for any incompressible, Newtonian fluid, Eq. (25) is of the form

$$0 = \partial_{\vec{r}} \cdot \mathbf{M} \partial_{\vec{r}} \mathbf{P}' - \partial_{\vec{r}} \cdot \vec{\mathbf{V}}. \quad (28)$$

In the present simple case, the matrix \mathbf{M} is constant and, in the usual coordinates, diagonal. The inhomogeneity $\vec{\mathbf{V}}$ (with dimensions of velocity) depends on time, x , and y . Equation (28) can be solved formally by the transformation

$$\partial_{\vec{r}} P' = \mathbf{M}^{-1} \left(\hat{z} \times \partial_{\vec{r}} G + \vec{\mathbf{V}} \right), \quad (29)$$

which requires a fundamental solution $G(x, y, t)$ satisfying

$$0 = \hat{z} \times \partial_{\vec{r}} \cdot \partial_{\vec{r}} P' = (\hat{z} \times \partial_{\vec{r}}) \mathbf{M}^{-1} (\hat{z} \times \partial_{\vec{r}}) G + (\hat{z} \times \partial_{\vec{r}}) \mathbf{M}^{-1} \vec{\mathbf{V}}. \quad (30)$$

With some rearrangements, Eq. (30) has the same simple structure as Eq. (28). The quantity G can be interpreted as a stream function generating a certain component of the large-scale variations of the velocity field $(v_x, v_y) \sim (\hat{z} \times \partial_{\vec{r}}) G$, the “singular mean flow” (in early works [59] expressed in terms of the vertical vorticity $-\nabla^2 G$). By using Eq. (30) instead of Eq. (28) and eliminating the pressure P' *via* Eqs. (29) also in the remaining equations [in our case (23,24)], a description fully in terms of the singular mean flow is obtained.

In principle the three forms (28,29,30) are equivalent, although the last is often preferred in the literature (for an overview see both Refs. [1,60]), perhaps because in some situations with high symmetry G is not excited, while P' is. When disregarding the effects of the additional soft mode φ' , application of the less obvious but direct method of Kaiser and Pesch [61] leads to the same result for the mean flow equation (30) as the route described here.

The flux $\vec{\mathbf{V}}$ in Eq. (29) is determined by Eq. (28) only up to a transformation $\vec{\mathbf{V}} \rightarrow \vec{\mathbf{V}} + (\hat{z} \times \partial_{\vec{r}}) G_0(x, y, t)$ which implies a redefinition $G \rightarrow G - G_0$. Hence $(\hat{z} \times \partial_{\vec{r}}) G$ is not generally proportional to the z average of the large scale flow. This is not necessary for the formalism to work. In simple cases, like the present, the stream function G has this property with the “natural” choice of $\vec{\mathbf{V}}$. To guarantee it in general, the method of Newell, Passot and Souli [60] can be used to derive Eq. (29) (Eq. (2.59) in [60]) directly under this additional constrain.

Here, following Ref. [1], the formulation as a mass conservation equation (28) is used, since it derives naturally from the general formalism and is thus easily extended to three spatial dimension, to additional homogeneous soft modes, or to relax the assumption of incompressibility (which is not essential for the relevance of mean flow as is sometimes suggested).

In principle, terms proportional to $\partial_x^2 \varphi'$, $\partial_y^2 \varphi'$ could also appear in the P' equation (25). It is a particularity of the system considered here that they do not. In the conduction regime of EC in cells with homeotropic boundary conditions it can be shown [58] that there is such a, presumably small, excitation of P' by φ' proportional to the dynamic flexoelectric coefficient ζ^E .

D. Variation of the boundary conditions

Of course, the reduction from 3D to 2D can also be carried out for other boundary conditions than (6,11). Some variants are of practical interest.

An effect similar to applying a magnetic field along y can be obtained by a homeotropic (normal) anchoring of the director at the boundaries: For negative, not too small ϵ_a , and with external electric fields as required for dielectric EC, a homeotropic director alignment is unstable and instead the director becomes planarly oriented everywhere, except for small boundary layers of thickness $(k_{11}/\epsilon_a)^{1/2}E_0^{-1} \approx \lambda$. Hence, on the length scales $\gg \lambda$ relevant for the amplitude formalism, the boundary layer vanishes and instead free boundary conditions for φ can be assumed. For this setup only some geometry factors have to be changed in Eqs. (10-25).

Another variant is a twisted cell, e.g. with $\varphi = 0$ at $z = -d/2$ and $\varphi = \pi/2$ at $z = d/2$, as it was recently investigated experimentally by Bohatsch and Stannarius [62]. Based on the reduced 3D description derived here, the linear theory for this configuration is developed in Ref. [63].

E. Higher order contributions

It is worth noticing that, when only the limit of small ϵ' is considered while keeping d fixed, there are several other nonlinear and higher order gradient terms besides those in lines (23c,23d) which are formally of the same order of magnitude. A longer list containing more than fifty terms has been calculated numerically by Kaiser and Pesch [61] for the conduction regime of EC. Their form correctly predicts the stability of ideal roll patterns close to threshold but, since it does not separate mean flow and director effects, is unable to describe important effects like the transition to abnormal rolls [64] (see Sec. VI A). These limitations are partly overcome in the less systematic but numerically surprisingly accurate description of Plaut and Pesch [40].

In fact, since the lowest order mean flow effects entering Eqs. (23-25) all depend on gradients of $|A'|^2$, they do not contribute to long-wavelength instabilities of the band center (i.e. $A \equiv \text{const.}$). For the calculation of the thresholds of long-wavelength instabilities of the pattern it may be useful to formally set up amplitude equations including higher order mean flow. But for a systematic quantitative description of *general* non-ideal patterns containing structures of size $\sim \lambda\epsilon^{-1/2}$ only the truncation used here is justified. When higher order mean flow becomes relevant the 2D amplitude formalism is already breaking down because, for example, the coherence length $\xi_y\epsilon^{-1/2}$ becomes of the order of the sample thickness [61].

VI. STABILITY OF IDEAL PATTERNS

Rather than deriving stability bounds of ideal patterns $A = a(z)\exp(iqx + ipy)$ using a reduced 2D description, it seems more appropriate to do the calculations directly based on the 3D equations, in particular when $H_y = 0$. This is easily seen from the fact that there is a (numerically small) manifest deviation of $a(z)$ from the $\cos(\pi z/d)$ profile at the threshold of all instabilities calculated below, indicating that the expansion for small A' is breaking down. Nevertheless, in order to obtain analytic estimates, Galerkin approximations will be used which correspond effectively to Eqs. (23-25) and their extension to higher order contributions. For simplicity, the stability analysis shall here be performed only at the band center $q, p = 0$ and only take homogeneous and long-wavelength instabilities with modulations along y into account. The latter restriction is justified by experimental observations and by the fact that, with this geometry, the advection of the pattern by mean flow is particularly strong. It is then sufficient to consider only the interaction of φ , v_x , and of the phase θ given by $A = a(z)\exp i\theta(y, z, t)$ [$a = a(z) = O(\epsilon'/g')^{1/2}$ be real and given by Eqs. (10,40b,40c)], which leads to the following linear problem:

$$\gamma_1 \partial_t \varphi = [(k_{11} + 2b e_-^2/\epsilon_a) \partial_y^2 + k_{22} \partial_z^2] \varphi - \alpha_3 \partial_y v_x + (q_c \Gamma/2) a^2 (\partial_y \theta - q_c \varphi), \quad (31a)$$

$$\rho_m \partial_t v_x = \eta_2 (\partial_y^2 + \partial_z^2) v_x + \alpha_3 \partial_y \partial_t \varphi + S_{yy} a^2 \partial_y (\partial_y \theta - q_c \varphi) + S_{zz} \partial_z (a^2 \partial_z \theta), \quad (31b)$$

$$\tau \partial_t \theta = -\tau q_c v_x + \beta_y \partial_y \varphi + \xi_y^2 \partial_y^2 \theta + \xi_z^2 a^{-2} \partial_z (a^2 \partial_z \theta). \quad (31c)$$

Since $a = 0$ at $z = \pm d/2$, the singular last term in Eq. (31c) implies boundary conditions $\partial_z \theta = 0$. The other boundary conditions are $\varphi, v_x = 0$ at $z = \pm d/2$.

A. Homogeneous destabilization

First, consider homogeneous ($\partial_y = 0$) destabilizations of the pattern. In this case φ decouples from v_x and θ . The destabilization of φ is known as the abnormal-roll instability and was investigated in the dielectric regime in Ref. [33]. It was found that

$$\epsilon' = \epsilon'_{AR} := -\frac{8 \pi^2 g' k_{33}}{3 d^2 q_c^2 \Gamma}, \quad (32)$$

which can be derived from Eqs. (23,24), is typically a good approximation of the threshold. In MBBA $\epsilon'_{AR} \approx 2.8 \times (\lambda/d)^2$ ($\omega\tau_0 \geq 8$). The value obtained by numerically calculating eigenmodes of Eq. (31a) directly is 3% lower than the value of Eq. (32). Below it will be shown that for MBBA the abnormal-roll instability is preceded by

a long-wavelength modulation instability. Nevertheless, some phenomena associated with abnormal rolls might be observable around $\varepsilon = \varepsilon_{AR}$, e.g. the tendency of defects in the convection pattern to cluster along lines parallel to the rolls.

For the discussion of homogenous perturbations of v_x and θ notice first the neutral mode associated with a translation of the pattern $\theta \rightarrow \theta + \text{const.}$. This mode is best dealt with by decomposing θ as $\theta = \tilde{\theta}(z, t) + \Theta(t)$ such that the z average $\langle \tilde{\theta} \rangle_z$ vanishes. By multiplying Eq. (31c) by a^2 and integrating over z the dynamics of Θ is obtained as

$$\partial_t \Theta = -q_c \frac{\langle a^2 v_x \rangle_z}{\langle a^2 \rangle_z}. \quad (33)$$

This describes the advection of the pattern by mean flow at large pattern amplitudes.

At the threshold of instability one has $\partial_t \tilde{\theta}, \partial_t v_x = 0$ and $\partial_t \Theta = \text{const.}$ ($\partial_t \Theta \neq 0$ implies an acceleration instability of pattern and liquid crystal). To calculate the threshold, eliminate $\tilde{\theta}$ from Eq. (31b) by Eqs. (31c,33), obtaining the equation

$$0 = \eta_2 \partial_z^2 v_x + \frac{S_{zz} \tau q_c}{\xi_z^2} a^2 \left[v_x - \frac{\langle a^2 v_x \rangle_z}{\langle a^2 \rangle_z} \right] \quad (34)$$

from which the critical mode can be determined numerically. When using the low-amplitude approximation $a^2 = (\varepsilon'/g') \cos^2(\pi z/d)$ the critical mode is found to be antisymmetric in z (i.e. $\partial_t \Theta = 0$) at

$$\varepsilon' = \varepsilon'_{\text{drift}} = 73.3 \frac{\eta_2 g' \xi_z^2}{d^2 S_{zz} \tau q_c}. \quad (35)$$

[With the large amplitude approximation $a^2 = \varepsilon/g$, the first symmetric and antisymmetric mode both become unstable at the *same* $\varepsilon = (4\pi^2 \eta_2 g \xi_z^2)/(d^2 S_{zz} \tau q_c)$.] The antisymmetric excitation of the phase $\tilde{\theta}$ involved in this instability is obviously inaccessible to a reduced 2D description. Since $S_{zz} < 0$ in MBBA, the value of $\varepsilon'_{\text{drift}} \approx -100 \times (\omega\tau_0)^{-1} (\lambda/d)^2$ is negative and the instability does not occur. However, since the electric contribution to S_{zz} [the second term in formula (A25)] is always positive and comparable in size with the hydrodynamic one, a positive S_{zz} is thinkable for other materials. When $S_{zz} < 0$, the mechanism leading to Eq. (34) is stabilizing – in particular for all perturbations of $\tilde{\theta}$: The lamellae of EC are forced to align normal to the boundaries. This explains why the experimental shadowgraph images, which average the pattern along z , remain quite sharp even for complicated pattern dynamics.

B. Modulation instabilities

The stability of ideal patterns with respect to perturbations in φ , v_x , and θ modulated with small wave numbers k along y was investigated numerically using the system (31). It was found that for MBBA the dominating

destabilizing feedback loop is based on the excitation of v_x by the term containing S_{yy} in Eq. (31b) and advection of the phase. There is a good Galerkin approximation for the numerical results. Using the low amplitude approximation for a^2 , Galerkin modes $\varphi, v_x \sim \cos(\pi z/d)$ and $\theta \sim 1$, and projectors $\int \cos(\pi z/d) \cdot \partial_z$ on Eqs. (31a,31b) and $\int \cos^2(\pi z/d) \cdot \partial_z$ on Eq. (31c) to reduce the system (31) to algebraic equations, the threshold for long-wavelength modulations instabilities is estimated to be at

$$\varepsilon' = \varepsilon'_{ZZ} := \frac{72\pi^4 \eta_2 g' k_{33} \xi_y^2}{d^2 q_c} \times \quad (36)$$

$$\left[512 k_{33} S_{yy} \tau - \eta_2 \Gamma (256 \beta_y + 27 \pi^2 q_c \xi_y^2) \right]^{-1}.$$

With $\beta_y = -q_c \xi_{yy}^2$ the parenthesis following Γ nearly vanish; the remainder is related to the small deviation of c_1 in Eq. (26a) from unity. Numerically $\varepsilon'_{ZZ} \approx 9 \times (\omega\tau_0)^{-1} (\lambda/d)^2$ (observe that ε'_{ZZ} and ε'_{AR} have different frequency dependence). In particular, at $\omega\tau_0 = 8$, using the second lowest Fourier approximation without flexoelectric effects, Eq. (36) yields $\varepsilon'_{ZZ} = 0.792 (\lambda/d)^2$ while the numerical solution of system (31) gives a threshold at $\varepsilon' = 0.797 (\lambda/d)^2$. Using the Galerkin approximation it is easily verified that the instability is in fact of the long-wavelength ($k \rightarrow 0$) type.

VII. QUALITATIVE TRANSITIONS

For the case $H_F = 0$, order of magnitude estimates shall be used to distinguish regions of qualitatively different pattern dynamics in parameter space – above as well as below the stability bounds of ideal patterns.

As mentioned before, simple Ginzburg Landau dynamics can be expected for small ϵ until the last two lines in Eq. (23) become relevant. Assuming $\partial_x \approx \varepsilon'^{1/2} \xi_x^{-1}$ and $|A'|^2 \approx \varepsilon'/g'$, these terms have an effect of the magnitude of $\varepsilon' A'$ when, say, $\varepsilon' \approx [3\pi^2 \eta_2 g q_c \xi_x \lambda^2]^2 / [(\pi^2 - 6)(S_E + S_x - S_z) \tau d^2]^2 \approx 2 \times 10^4 \times (\lambda/d)^4 (\omega\tau_0)^{-2}$ (MBBA, $\omega\tau_0 \gtrsim 10$). Preliminary simulations of Eqs. (23,25) with $\varphi \equiv 0$ show that for higher ε' defect cores (where $\partial_x |A'|^2$ is large) are strongly deformed and lines along which the phase $\arg A'$ “jumps” are often generated and long living (rather long living phase jump lines are also observed experimentally and in simulations of a similar model [61]; it is not clear, though, whether these are due to lowest order mean flow effects). But the simulations also indicate that these lowest order mean flow effects, although they are formally dominating over the direct nonlinear saturation *via* the last term in line (23b), do not prevent the system from finally reaching a steady state with $|A'|^2 \approx \varepsilon'/g'$.

Thus, assuming still $|A'|^2 \approx \varepsilon'/g'$, there will be a further transition at $\varepsilon' \approx [3^{1/2} \pi (\alpha_4 +$

$2\eta_2)gk_{33}q_c^3\xi_y/(128\alpha_2S_x)]^{2/3} \times (\lambda/d)^{8/3} \approx 1. \times (\lambda/d)^{8/3}$ (MBBA, $\omega\tau_0 \geq 8$) where contributions from slaved excitations of the in-plane director φ by mean flow become relevant in the 2D pattern dynamics. Semiquantitatively these effects are described by Eq. (24) with $H_y = 0$, but a restriction of dynamics to a single linear mode of φ is then not justified.

When, with increasing ϵ , horizontal length scales become of the size of the sample thickness d [at $\epsilon' \approx (\pi\xi_x/d)^2 \approx 0.2 \times (\lambda/d)^2$ (MBBA), say] the 2D description breaks down. Because then d is not the dominating length scale for the damping of mean flow anymore, the trend in the influence of mean flow on the smallest structures in the A field (e.g. defects) is reversed. Now the structures themselves set the length scale. Assuming $\partial_x \approx \epsilon^{1/2}\xi_x^{-1}$ and $|A|^2 \approx \epsilon/g$, the contribution $i\tau v_x A$ in Eq. (10) is large compared to ϵA up to $\epsilon \approx (q_c S_x \tau \xi_x / \eta_2 g)^2 \approx 1. \times 10^{-6} \times (\omega\tau_0)^2$ (MBBA, $\omega\tau_0 \gtrsim 10$). For larger ϵ the cores of defects are not affected by lowest order mean flow effects. Larger structures, like the phase field of the pattern or variations in the defect density (e.g. in chevron patterns), may still be.

Current experimental resolutions are of the order $\Delta\epsilon = 10^{-3} \dots 10^{-2}$. The estimates above suggest that lowest order mean flow effects are best observed near the upper limit of the frequency range for the validity of the hydrodynamic description used here, at $\omega\tau_0 = O(10^2)$ (see Section II C). With $d \approx 5\lambda$ they should be observable in the range of validity of the 2D description.

According to the model for the chevron mechanism [65], chevrons depend essentially on the abnormal-roll mechanism and can only form above the abnormal-roll instability bound [here given by Eq. (32)]. Thus, it is plausible to assume a $\epsilon' \sim (\lambda/d)^2$ threshold for chevron formation, in accordance with measurements presented in Ref. [23], where an approximate ω^{-1} frequency dependence is found.

For very high ϵ' many authors report the formation of disclination loops, which, being singularities in the director field, indicate already a breakdown of *hydrodynamics*. In thicker cells, the chevron pattern might decay along other routes before the 3D amplitude formalism breaks down at some $\epsilon = O(1)$.

For convection in most quasi-2D systems, i.e. systems with $d/\lambda = O(1)$, all these transitions, from the breakdown of simple 2D Ginzburg-Landau dynamics to the breakdown of the amplitude formalism, do, in principle, collapse at $\epsilon = O(1)$. Only by specially designed experiments (as in [66]) can these transitions be unfolded.

VIII. ELECTRIC NusSELT NUMBERS

Recently “electric Nusselt numbers” $\mathcal{N}_r, \mathcal{N}_i$ have been introduced by Gleeson, Gheorghiu, Plaut [67] as the ratio of the in-phase or, respectively, out-of-phase components of the electric current to the corresponding values

expected for the unstructured basic state at a given voltage, minus one. As for the Nusselt number in thermal convection, they are to first approximation proportional to $|A|^2$.

Several interesting questions can be addressed by measuring electric Nusselt numbers. First, it follows from the discussion above that, in dielectric EC, $|A|^2 \approx \epsilon/g$ for thick enough cells even far inside the three-dimensionally chaotic range (the average of $|A|^2$ across the pattern is typically only weakly reduced in the presence of defects; see, e.g., Ref. [65]). Measurements of the electric Nusselt numbers therefore seem to be an effective method to test an essential feature of the theory. Second, Nusselt number measurements may also help to identify the qualitative changes in the dynamics predicted in Section VII, in particular since they do, in contrast to optical methods, not lose their sensitivity in thick cells or with small wavenumbers. Finally, the frequency dependence of the Landau coefficient g' , which enters the Nusselt numbers near threshold in a simple way, provides information on the strength of the dynamic flexoelectric effect (see Appendix A). From the derivation of g' it is clear that boundary effects do not interfere in these measurements. To obtain the theoretical value for the Nusselt numbers, take the x and y average (symbol $\langle \cdot \rangle_{xy}$) of Eq. (40b) plus i times Eq. (40c), which leads to

$$\begin{aligned} (\sigma_{\perp} + i\omega\epsilon_{\perp}) \partial_z^2 \langle \Phi_r + i\Phi_i \rangle_{xy} = \\ (I_r + iI_i) \partial_z \langle |A|^2 \rangle_{xy} \\ + (I_{rz} + iI_{iz}) \partial_z \langle \text{Im}\{A^* \partial_x A\} \rangle_{xy}. \end{aligned} \quad (37)$$

Taking the boundary conditions (6,11) into account, this implies, similar as for $\Phi_r^{(2)} + i\Phi_i^{(2)}$ in Eq. (18),

$$\begin{aligned} \frac{1}{2}j_z := -(\sigma_{\perp} + i\omega\epsilon_{\perp}) \partial_z \langle \Phi_r + i\Phi_i \rangle_{xy} = \\ (I_r + iI_i) \langle |A|^2 \rangle_{xyz} \\ + (I_{rz} + iI_{iz}) \langle \text{Im}\{A^* \partial_x A\} \rangle_{xyz} \end{aligned} \quad (38)$$

at $z = \pm d/2$. Obviously, j_z is the complex amplitude of the average, pattern-induced electric current density through the sample. (The last term on the r.h.s. represents a correction due to a global deviation of the average wavenumber from the critical one, and will be dropped below.) Thus,

$$\mathcal{N}_r = \frac{2I_r \langle |A|^2 \rangle_{xyz}}{E_0\sigma_{\perp}} \quad (39a)$$

and

$$\mathcal{N}_i = \frac{2I_i \langle |A|^2 \rangle_{xyz}}{E_0\epsilon_{\perp}\omega}. \quad (39b)$$

At threshold, $(d/d\epsilon') \langle |A|^2 \rangle_{xyz} = (2g')^{-1}$, e.g. $d\mathcal{N}_r/d\epsilon' = 0.31$ in MBBA at $\omega\tau_0 = 8$, dropping flexoelectric contributions. The value increases roughly $\sim \omega$ as frequency

increases. Typically, it seems to be larger than the corresponding value for the conduction regime [67].

IX. CONCLUSION

It has been shown how the 3D dielectric convection pattern interacts with various homogeneous soft modes, which are related to undamped hydrodynamic modes. The method to establish these relations is not unique, but the “center manifold” method seems to be favorable over the “order parameter” method.

The reduction of the 3D pattern dynamics to a quasi-2D form in the layer geometry was derived analytically, thus establishing a description of the interaction of the pattern with the twist mode and the pressure field (or singular mean flow). Scaling analysis suggests that the transition from the simple, quasi-2D Ginzburg-Landau dynamics to manifestly 3D dynamics in thick layers unfolds into several well distinguished steps, the first of which occurs already very close to threshold ($\epsilon' = O(\lambda/d)^4$).

These characteristics should generally be expected for 3D patterns.

Ideal, dielectric EC patterns are found to destabilize at some value $\epsilon' \sim (\omega\tau_0)^{-1}(\lambda/d)^2$ for which an analytic approximation in terms of material parameters is given. A particular nonlinear mechanism that stabilizes the phase of the pattern to be constant along z , thus giving the pattern a 2D appearance also at higher ϵ' , is identified in Sec. VI. As outlined in Sec. VIII, measurements of the electric Nusselt numbers are suitable for quantitatively testing the theory, probing the dynamic flexoelectric effect in nematic liquid crystals independent of boundary effects, and investigating the route of the transition from simple 2D to fully 3D dynamics.

It is my pleasure to thank L. Kramer, Y. Kuramoto, A. Lindner, W. Pesch, and E. Plaut for valuable discussion, W. Decker and W. Pesch for providing the basic nematodynamic equations in a computer readable form, the Kyoto University for its hospitality and the Japan Foundation for the Promotion of Science (P98285) and the Ministry of Education, Science, Sports and Culture in Japan for their support.

$$0 = - [(\sigma_{\parallel} - 2b\sigma_a) \partial_x^2 + \sigma_{\perp} (\partial_y^2 + \partial_z^2)] \Phi_0 - 2b e_- (\sigma_a/\epsilon_a) \partial_x \partial_y \varphi \quad (40a)$$

$$0 = + E_0 \partial_x^2 [\epsilon_{\parallel} \omega \Phi_i - (\sigma_{\parallel} - \sigma_a) \Phi_r] + E_0 (\partial_y^2 + \partial_z^2) (\epsilon_{\perp} \omega \Phi_i - \sigma_{\perp} \Phi_r) - [\sigma_a/\epsilon_a + (1 - 3b) E_0^2 \epsilon_a/2 \gamma_1] (e_+ - 2\gamma_1 \zeta^E) \partial_x^2 \partial_z \Phi_0 + [(\sigma_a/\epsilon_a) (-k_{11} + k_{22}) + e_- E_0^2 (1 - 3b) (e_+/2\gamma_1 - \zeta^E)] \partial_x \partial_y \partial_z \varphi \quad (40b)$$

$$+ (\sigma_a/\epsilon_a) \partial_x (\alpha_3 \partial_z v_x + \alpha_2 \partial_x v_z) + E_0 (I_r \partial_z |A|^2 + I_{rx} \partial_x \text{Im}\{A^* \partial_z A\} + I_{rz} \partial_z \text{Im}\{A^* \partial_x A\}) 0 = - E_0 \partial_x^2 [\sigma_{\parallel} \Phi_i + (\epsilon_{\parallel} - \epsilon_a) \omega \Phi_r] - E_0 (\partial_y^2 + \partial_z^2) (\sigma_{\perp} \Phi_i + \epsilon_{\perp} \omega \Phi_r) - \omega (1 - 2b) (e_+ - 2\gamma_1 \zeta^E) \partial_x^2 \partial_z \Phi_0 + [\omega (-k_{11} + k_{22}) - (2b e_-/\epsilon_a) (e_+ - 2\gamma_1 \zeta^E)] \partial_x \partial_y \partial_z \varphi + \omega \partial_x (\alpha_3 \partial_z v_x + \alpha_2 \partial_x v_z) + E_0 (I_i \partial_z |A|^2 + I_{ix} \partial_x \text{Im}\{A^* \partial_z A\} + I_{iz} \partial_z \text{Im}\{A^* \partial_x A\}) \quad (40c)$$

$$\gamma_1 \partial_t \varphi = [k_{33} \partial_x^2 + (k_{11} + 2b e_-^2/\epsilon_a) \partial_y^2 + k_{22} \partial_z^2 + \chi_a H_y^2] \varphi + (e_+ - 2\gamma_1 \zeta^E - 2b e_-) \partial_x \partial_y \Phi_0 - \alpha_3 \partial_y v_x - \alpha_2 \partial_x v_y + (q_c \Gamma/2) \text{Im}\{A^* (\partial_y - iq_c \varphi) A\} \quad (40d)$$

$$\rho_m \partial_t v_x = (\alpha_1 + \alpha_4 + \alpha_5 + \alpha_6) \partial_x^2 v_x + \eta_2 (\partial_y^2 + \partial_z^2) v_x + (\alpha_2 + \eta_1) \partial_x (\partial_y v_y + \partial_z v_z) + \partial_x [-P - E_0 \epsilon_{\perp} \partial_z \Phi_r + 2\alpha_3 \zeta^E (\partial_y^2 + \partial_z^2) \Phi_0] + \alpha_3 \partial_y \partial_t \varphi + S_x \partial_x |A|^2 + S_{xx} \partial_x \text{Im}\{A^* \partial_x A\} + S_{yy} \partial_y \text{Im}\{A^* (\partial_y - iq_c \varphi) A\} + S_{zz} \partial_z \text{Im}\{A^* \partial_z A\} \quad (40e)$$

$$\rho_m \partial_t v_y = (\eta_1 \partial_x^2 + \alpha_4 \partial_y^2 + \alpha_4 \partial_z^2/2) v_y + \partial_y [(\alpha_2 + \eta_1) \partial_x v_x + \alpha_4 \partial_z v_z/2] + \partial_y [-P - E_0 \epsilon_{\perp} \partial_z \Phi_r + 2\alpha_2 \zeta^E \partial_x^2 \Phi_0] + \alpha_2 \partial_x \partial_t \varphi + S_{xy} \partial_x \text{Im}\{A^* (\partial_y - iq_c \varphi) A\} \quad (40f)$$

$$\rho_m \partial_t v_z = [(\alpha_2 + \eta_1) \partial_x^2 + \alpha_4 (\partial_y^2/2 + \partial_z^2)] v_z + \partial_z [(\alpha_3 + \alpha_2 + \eta_1) \partial_x v_x + \alpha_4 \partial_y v_y/2] + \partial_z [-P - (k_{11} - k_{22} + 2b e_+ e_-/\epsilon_a) \partial_x \partial_y \varphi] - [e_+ - 2b e_+ - 2(\gamma_1 + \alpha_2) \zeta^E] \partial_x^2 \partial_z \Phi_0 - E_0 [(\epsilon_{\parallel} - \epsilon_a) \partial_x^2 + \epsilon_{\perp} \partial_y^2 + 2\epsilon_{\perp} \partial_z^2] \Phi_r + S_z \partial_z |A|^2 + S_{xz} \partial_x \text{Im}\{A^* \partial_z A\} + S_{zx} \partial_z \text{Im}\{A^* \partial_x A\} \quad (40g)$$

$$0 = \nabla \cdot \vec{v} \quad (40h)$$

(Note: L^AT_EX is confused here, so we continue with a single column)

APPENDIX A: RESULTS FOR LINEAR STABILITY AND COUPLING COEFFICIENTS IN 3D

Some analytic and numeric results relating the 3D description of the pattern dynamics to hydrodynamics are presented here, in particular analytic approximations for all coefficients entering the the results in Sections V, VI, and VIII. In the second lowest Fourier approximation the onset of dielectric EC is at

$$E_c^2 = \frac{4 \omega \sigma_{\parallel} (\alpha_2^2 - \gamma_1 \eta_1)}{X \left(\alpha_2 - \frac{2 \omega \sigma_{\parallel} (\alpha_2 \epsilon_{\parallel} + \epsilon_a \eta_1)}{4 \epsilon_{\parallel}^2 \omega^2 + \sigma_{\parallel}^2} \right) - \epsilon_a \eta_1 \sigma_{\perp}} \quad (\text{A1})$$

with a critical wavenumber

$$q_c^2 = \frac{2 \omega (-\alpha_2^2 + \gamma_1 \eta_1)}{k_{33} \eta_1} \times \frac{2 \epsilon_{\parallel}^2 \omega^2 + \sigma_{\parallel}^2 - \frac{2 \epsilon_a \epsilon_{\parallel} \epsilon_{\perp} \eta_1 \omega^2 \sigma_{\parallel}}{\alpha_2 X - \epsilon_a \eta_1 \sigma_{\perp}}}{4 \epsilon_{\parallel}^2 \omega^2 + \sigma_{\parallel}^2 - \frac{2 X \omega \sigma_{\parallel} (\alpha_2 \epsilon_{\parallel} + \epsilon_a \eta_1)}{\alpha_2 X - \epsilon_a \eta_1 \sigma_{\perp}}}, \quad (\text{A2})$$

where $X := \epsilon_{\parallel} \sigma_a - \epsilon_a \sigma_{\parallel}$. The accurate numerical result for E_c^2 vs. ω is nearly a perfect straight line (see Fig. 2), which can probably be understood by means of the approximation used in [18]. Formula (A1) nicely estimates the offset of this line for intermediate $\omega \tau_0$, but gives a different slope as $\omega \tau_0 \rightarrow \infty$. The deviations at the lower end are an artifact occurring with all truncated Fourier approximations. For q_c^2 the situation is similar.

In the second lowest Fourier approximation, the excitation of the hydrodynamic fields in the convection pattern near threshold (critical mode) is

$$\Phi = |A| \sin(q_c x + \arg A) \times (\Phi_u + 2 \Phi_c \cos(2 \omega t) - 2 \Phi_s \sin(2 \omega t)), \quad (\text{A3})$$

$$n_z = 2 |A| \cos(q_c x + \arg A) (\cos(\omega t) + \sin(\omega t)), \quad (\text{A4})$$

$$f = 2 |A| \sin(q_c x + \arg A) \times (f_c \cos(\omega t) - f_s \sin(\omega t)), \quad (\text{A5})$$

where f generates a velocity field $\vec{v} = (\partial_x \partial_z, \partial_y \partial_z, -\partial_x^2 - \partial_y^2) f$ and the real constants $f_c, f_s, \Phi_u, \Phi_c, \Phi_s$ are given

by

$$4\eta_1 f_c q_c^3 = -4\alpha_2 \omega + \frac{X E_c^2 (8\epsilon_{\parallel}^2 \omega^2 - 2\epsilon_{\parallel} \omega \sigma_{\parallel} + 3\sigma_{\parallel}^2)}{4\epsilon_{\parallel}^2 \omega^2 \sigma_{\parallel} + \sigma_{\parallel}^3}, \quad (\text{A6})$$

$$4\alpha_2 f_s q_c^3 = -\epsilon_a E_c^2 - 4\gamma_1 \omega + 4k_{33} q_c^2 + \frac{\epsilon_a E_c^2 [2\epsilon_a \omega (2\epsilon_{\parallel} \omega - \sigma_{\parallel}) + \sigma_a (2\epsilon_{\parallel} \omega + \sigma_{\parallel})]}{4\epsilon_{\parallel}^2 \omega^2 + \sigma_{\parallel}^2}, \quad (\text{A7})$$

$$\Phi_u = \frac{E_c \sigma_a}{q_c \sigma_{\parallel}}, \quad (\text{A8})$$

$$\Phi_c + i\Phi_s = \frac{(1-i) E_c (2i\epsilon_a \omega + \sigma_a)}{2 q_c (2i\epsilon_{\parallel} \omega + \sigma_{\parallel})}. \quad (\text{A9})$$

With the help of the real constants Φ_u^+ , Φ_c^+ , Φ_s^+ , n_z^+ which characterize the adjoint eigenvector

$$\Phi_u^+ = \frac{E_c (\alpha_2 \epsilon_{\parallel} + \epsilon_a \eta_1) q_c}{2 \alpha_2 \sigma_{\parallel}}, \quad (\text{A10})$$

$$\Phi_c^+ + i\Phi_s^+ = \frac{q_c}{4\alpha_2 X E_c \omega} \times \left\{ +E_c^2 [-\alpha_2 X + \epsilon_a \eta_1 (2i\epsilon_{\perp} \omega + \sigma_{\perp})] - 4 [(\alpha_2^2 - \gamma_1 \eta_1) \omega + k_{33} \eta_1 q_c^2] (2i\epsilon_{\parallel} \omega + \sigma_{\parallel}) \right\}, \quad (\text{A11})$$

$$n_z^+ = -\frac{\eta_1 q_c^2}{\alpha_2} \quad (\text{A12})$$

and the normalization factor

$$4N = 2(q_c^2 - n_z^+) \epsilon_a E_c^2 + E_c q_c [(\epsilon_a n_z^+ - \epsilon_{\parallel} q_c^2) (\Phi_u + \Phi_c + \Phi_s) - 2\epsilon_a \omega (\Phi_c^+ + \Phi_s^+) - \sigma_a (2\Phi_u^+ + \Phi_c^+ - \Phi_s^+)], \quad (\text{A13})$$

analytic results for most coupling coefficients entering the 3D description can be obtained:

$$2N\tau = \epsilon_a E_c (2\Phi_u^+ + \Phi_c^+ - \Phi_s^+) q_c - 2\epsilon_{\parallel} (\Phi_u^+ \Phi_u + \Phi_c^+ \Phi_c + \Phi_s^+ \Phi_s) q_c^2, \quad (\text{A14})$$

$$\begin{aligned} E_c^2 \xi_x^2 = & 8k_{33}\eta_1 \left\{ -6k_{33}\eta_1 q_c^2 \sigma_{\parallel} \left(4\epsilon_{\parallel}^2 \omega^2 + \sigma_{\parallel}^2 \right) + E_c^2 \left[\epsilon_a \eta_1 \left(2\epsilon_{\parallel} \epsilon_{\perp} \omega^2 \sigma_{\parallel} + 2\epsilon_{\parallel}^2 \omega^2 \sigma_{\perp} + \sigma_{\parallel}^2 \sigma_{\perp} \right) - \alpha_2 \left(2\epsilon_{\parallel}^2 \omega^2 + \sigma_{\parallel}^2 \right) X \right] \right\} \\ & \times \left\{ 8 \left[2\epsilon_{\parallel} k_{33}\eta_1 (\alpha_2 \epsilon_{\parallel} - \epsilon_a \eta_1) \omega^2 q_c^2 + (\alpha_2 \epsilon_{\parallel} + \epsilon_a \eta_1) (\alpha_2^2 - \gamma_1 \eta_1) \omega^2 \sigma_{\parallel} + \alpha_2 k_{33}\eta_1 q_c^2 \sigma_{\parallel}^2 \right] X + 3\alpha_2^2 E_c^2 \sigma_{\parallel} X^2 \right. \\ & \left. - 8\epsilon_a k_{33}\eta_1^2 q_c^2 \left(4\epsilon_{\parallel}^2 \omega^2 + \sigma_{\parallel}^2 \right) \sigma_{\perp} + E_c^2 \left[\epsilon_a^2 \eta_1^2 \left(4\epsilon_{\perp}^2 \omega^2 \sigma_{\parallel} + 8\epsilon_{\parallel} \epsilon_{\perp} \omega^2 \sigma_{\perp} + 3\sigma_{\parallel} \sigma_{\perp}^2 \right) - 2\alpha_2 \epsilon_a \eta_1 \left(4\epsilon_{\parallel} \epsilon_{\perp} \omega^2 + 3\sigma_{\parallel} \sigma_{\perp} \right) X \right] \right\}^{-1}, \quad (\text{A15}) \end{aligned}$$

$$\begin{aligned} 2N\xi_y^2 = & \epsilon_{\perp} E_c (\Phi_u + \Phi_c + \Phi_s) q_c - (f_c + f_s) \alpha_4 q_c^3 \\ & - 4\epsilon_{\perp} \omega (\Phi_s^+ \Phi_c - \Phi_c^+ \Phi_s) - 2\sigma_{\perp} (\Phi_u^+ \Phi_u + \Phi_c^+ \Phi_c + \Phi_s^+ \Phi_s) + \text{flexo}, \quad (\text{A16}) \end{aligned}$$

$$\begin{aligned} 2N\xi_z^2 = & \epsilon_{\perp} E_c (\Phi_u + \Phi_c + \Phi_s) q_c + 4\alpha_3 \omega - 2(f_c + f_s) (\alpha_1 + \alpha_3 + \alpha_4 + \alpha_5 + (\alpha_3/\alpha_2) \eta_1) q_c^3 \\ & - 4\epsilon_{\perp} \omega (\Phi_s^+ \Phi_c - \Phi_c^+ \Phi_s) - 2\sigma_{\perp} (\Phi_u^+ \Phi_u + \Phi_c^+ \Phi_c + \Phi_s^+ \Phi_s) + \text{flexo}, \quad (\text{A17}) \end{aligned}$$

$$\begin{aligned} (8/3)Ng = & (2q_c^2 - 4n_z^+) \epsilon_a E_c^2 + 4q_c^2 [\omega (\alpha_3 + \gamma_2) - 2\epsilon_a n_z^+ \Phi_u \Phi_c] \\ & + (f_c + f_s) [(6\alpha_2 + 4\alpha_3) n_z^+ - 4(\alpha_1 + \gamma_2) q_c^2] q_c^3 - 2E_c q_c \sigma_a (3\Phi_u^+ + \Phi_c^+ - 2\Phi_s^+) \\ & + \epsilon_a E_c q_c [(5n_z^+ - 2q_c^2) (\Phi_u + 2\Phi_c) - 4\omega (2\Phi_c^+ + \Phi_s^+)] + 8\omega q_c^2 \epsilon_a (\Phi_c^+ \Phi_u + 2\Phi_s^+ \Phi_c - 2\Phi_c^+ \Phi_s) \\ & + 4q_c^2 \sigma_a [2\Phi_u^+ (\Phi_u - \Phi_s) + 2\Phi_c^+ \Phi_c + \Phi_s^+ (2\Phi_s - \Phi_u)] + \text{flexo}, \quad (\text{A18}) \end{aligned}$$

$$\begin{aligned} 4I_r + 4iI_i = & (i\epsilon_a \omega + \sigma_a) [(4 - 2i) E_c - (2 - 2i) q_c (\Phi_u + i\Phi_c - \Phi_s)] \\ & + q_c^3 \epsilon_a E_c [(-3 + i) f_c + (1 - i) f_s] + 2\epsilon_{\parallel} q_c^4 [f_c (\Phi_u + \Phi_c + i\Phi_s) + i f_s (\Phi_u - \Phi_c - i\Phi_s)], \quad (\text{A19}) \end{aligned}$$

$$\begin{aligned} 4I_{rx} + 4iI_{ix} = & \frac{2(i\epsilon_a \omega + \sigma_a)}{\epsilon_a E_c} \times \\ & \left[4\gamma_2 (f_c - f_s) q_c^2 + 2\epsilon_a E_c (\Phi_u + \Phi_c - \Phi_s) - \epsilon_a (\Phi_u^2 + 2\Phi_c^2 + 2\Phi_s^2) q_c + 4q_c (k_{33} - k_{11}) \right] \\ & - (2 - 2i) (i\epsilon_a \omega + \sigma_a) (\Phi_u + i\Phi_c - \Phi_s) - q_c^2 \epsilon_a E_c [(-3 + i) f_c + (1 - i) f_s] \\ & - 2\epsilon_{\parallel} q_c^3 [f_c (\Phi_u + \Phi_c + i\Phi_s) + i f_s (\Phi_u - \Phi_c - i\Phi_s)] + \text{flexo}, \quad (\text{A20}) \end{aligned}$$

$$\Gamma = 4k_{22} - 4k_{33} - \epsilon_a (E_c/q_c) (\Phi_u + \Phi_c - \Phi_s) + \epsilon_a (\Phi_u^2 + 2\Phi_c^2 + 2\Phi_s^2) - 2\alpha_3 q_c (f_c - f_s) + \text{flexo}. \quad (\text{A21})$$

$$2S_x = q_c [2q_c^2 (\alpha_1 + \alpha_5 + \gamma_2) (f_c - f_s) - \epsilon_a E_c (\Phi_u + \Phi_c - \Phi_s) + q_c \epsilon_{\parallel} (\Phi_u^2 + 2\Phi_c^2 + 2\Phi_s^2)], \quad (\text{A22})$$

$$2S_z = 2\alpha_5 q_c^3 (f_c - f_s) + \epsilon_a E_c [2E_c - q_c (\Phi_u + \Phi_c - \Phi_s)], \quad (\text{A23})$$

$$2S_{yy} = (2\eta_2 - \alpha_4) (f_c - f_s) q_c^2 + q_c \epsilon_{\perp} (\Phi_u^2 + 2\Phi_c^2 + 2\Phi_s^2) + \text{flexo}, \quad (\text{A24})$$

$$2S_{zz} = 2(\gamma_2 - \alpha_1) (f_c - f_s) q_c^2 + q_c \epsilon_{\perp} (\Phi_u^2 + 2\Phi_c^2 + 2\Phi_s^2) + \text{flexo}, \quad (\text{A25})$$

$$2S_{xy} = (\alpha_2 + \alpha_5) (f_c - f_s) q_c^2 - \epsilon_a E_c (\Phi_u + \Phi_c - \Phi_s) + q_c \epsilon_{\parallel} (\Phi_u^2 + 2\Phi_c^2 + 2\Phi_s^2) + \text{flexo}, \quad (\text{A26})$$

$$2S_{xz} = 2(\gamma_2 - \alpha_1) (f_c - f_s) q_c^2 + q_c \epsilon_{\perp} (\Phi_u^2 + 2\Phi_c^2 + 2\Phi_s^2) + 4q_c (k_{33} - k_{11}) + \text{flexo}, \quad (\text{A27})$$

Here ‘‘flexo’’ stands for flexoelectric corrections, which involve matrix inversions and are hard to express in a compact form. For similar reasons, no formulas are given for κ_x , S_{xx} , S_{zx} , I_{rz} and I_{iz} . The coefficients κ_z vanishes for the second lowest Fourier approximation (and $\rho_m = 0$) and α_x and $\beta_y + q_c \xi_y^2$ have only flexoelectric contributions. The expression for ξ_x^2 has a different structure than the other formulas because it was not calculated with the ‘‘center manifold’’ formalism but by differentiating the determinantal condition for stability of the basic state, which is more effective in this case. There are indirect contributions from excitations of n_z entering S_{xz} ,

I_{ix} and I_{rx} [the bracket in Eq. (A20), in Eq. (A27) they cancel favorably]. These have been calculated only in the lowest Fourier approximation (i.e. for the non-oscillatory part of n_z), which introduces a small error.

The quality of these results can be judged by comparing the values obtained for MBBA at $\omega\tau_0 = 8$ with the accurate numerical values in Table I (only the approximation for the indirect contribution from n_z entering S_{xz} , I_{ix} and I_{rx} is retained). In the combinations in which the results are expressed there, they are, for fixed $\omega\tau_0$, independent of the electric conductivity and, with the exception of κ_x , κ_z , I_{rx} , and some contributions involving ζ'^E , also largely independent of $\omega\tau_0$ for $\omega\tau_0 > 8$.

Two exceptions, which should both be experimentally accessible, shall be highlighted: the dynamic flexoelectric contribution to $E_c \alpha_x$, which increases linear in $\omega \tau_0$, and the contribution to g proportional to ζ'^{E^2} which is the only one which increases $\sim (\omega \tau_0)^2$ as $\omega \tau_0 \rightarrow \infty$. The result for g in the lowest Fourier approximation

$$g = 9.45 + 0.00252 e_+^2 - 0.00401 \omega \tau_0 e_+ \zeta'^E - 5.18 \times 10^{-5} \omega \tau_0 \zeta'^{E^2} + 0.00102 \omega^2 \tau_0^2 \zeta'^{E^2} \quad (\text{A28})$$

illustrates the latter effect, although it is correct only in its order of magnitude. The flexoelectric contributions in Eq. (A28) and also in Table I are expressed in terms of $e_+ := e_1 + e_3$, $e_- := e_1 - e_3$, and $\zeta'^E := 2\gamma_1 \zeta^E$, in units of 10^{-12}Cm^{-1} ($3.00 \times 10^{-5} \text{dyn}^{1/2}$ in Gaussian units). Typical values measured for e_1 and e_3 are a few times that much (see the overviews in Refs. [68,16]).

As a result of the approximate $\pi/4$ phase shift of the director oscillations, κ_z is so small that the remaining finite viscous effect is comparable in size to the effect of finite mass density ρ_m , which has been suppressed everywhere else.

APPENDIX B: “ORDER PARAMETER” VS. “CENTER MANIFOLD” METHOD

Here, two general methods for obtaining amplitude equations are compared. It is shown that they give different results in the presence of multiple homogeneous soft modes. In this work, the “center manifold” method is used to derive the reduced equations. In order to keep the formalism simple, it will be restricted to homogeneous ($\vec{q} = 0$) modes and their slow modulations. The inclusion of patterning soft modes ($|\vec{q}| \neq 0$) is straight forward.

1. Formal setting

Let the state vector $U(\vec{r})$ describe the configuration of all relevant degrees of freedom (e.g. hydrodynamic fields) of the system in the (ideally) infinitely extended, D -dimensional \vec{r} space. Assume the “microscopic equations” to be of the form

$$0 = F(U) = L(\partial_t, \nabla)U(\vec{r}) + \text{nonlinear terms}, \quad (\text{B1})$$

where the linear operator $L(\partial_t, \nabla)$ is polynomial in ∂_t and ∇ , acting on $U(\vec{r})$ locally and translation invariant in space and time. There are several branches j of linear modes $V_j(\vec{q})$ which solve the generalized eigenvalue problem

$$L(\sigma_j(\vec{q}), i\vec{q})V_j(\vec{q}) = 0, \quad (\text{B2})$$

and, with some suitable scalar product $\langle \cdot | \cdot \rangle$ (which does *not* contain an integration over \vec{r}), adjoint eigenstates

$$W_j(\vec{q})L(\sigma_j(\vec{q}), i\vec{q}) = 0. \quad (\text{B3})$$

For some branches $j \in K$ the growth rates $\text{Re}\{\sigma_j(\vec{q})\}$ vanish (or are small) at their maxima at $\vec{q} = 0$, for the others ($j \notin K$) they are negatively large in the vicinity of $\vec{q} = 0$.

2. The order parameter method

Using the “order parameter” method physical states are characterized by weighted sums over slow eigenfunctions of $L(\partial_t, \nabla)$,

$$U(\vec{r}) = \sum_{j \in K} \int_{\Omega} u_j(\vec{q}) V_j(\vec{q}) \exp(i\vec{q} \cdot \vec{r}) d\vec{q} + R(\{u_k\}). \quad (\text{B4})$$

The weights $u_j(\vec{q})$ are interpreted as the Fourier transforms of the set of “amplitudes” used in the reduced description. The range of integration Ω is a region around $\vec{q} = 0$, large enough to include all significant contributions from $u_j(\vec{q})$ and small enough to exclude slow (patterning) modes at large wavenumbers. With this ansatz slaved contributions $R(\{u_k\})$, which are fully in the fast eigenspace of L , come in only at nonlinear order. The linear dynamics for each amplitude is simply given by

$$\partial_t u_j(\vec{q}) = \sigma_j(\vec{q}) u_j(\vec{q}). \quad (\text{B5})$$

An inverse Fourier transform yields the linear dynamics in physical space, which is usually simplified by truncating the Taylor expansion of $\sigma_j(\vec{q})$ in each component of \vec{q} for small $|\vec{q}|$, such that, in physical space, derivatives of u_j are obtained.

However, the situation is different in the case of multiple slow branches. Then $\sigma_j(\vec{q})$ is typically non-analytic in the components of \vec{q} (although it is analytic in $|\vec{q}|$). As a generic example, consider the linear operator

$$L(\partial_t, \nabla) = \begin{pmatrix} \partial_x^2 + \partial_y^2 - \partial_t & \partial_x \partial_y \\ \partial_x \partial_y & \partial_x^2 + \partial_y^2 - a \partial_t \end{pmatrix} \quad (\text{B6})$$

with a positive parameter a . There are two neutral modes at $(q, p) := \vec{q} = 0$. It is easily seen that one of the two growth rates is of the form

$$\sigma_1(q, p) = -\frac{p^4 + p^2 q^2 + q^4}{p^2 + q^2} + O(a), \quad (\text{B7})$$

i.e., non-analytic at $q, p = 0$. As a result, the corresponding amplitude equation in physical space

$$\begin{aligned} \partial_t u_1(\vec{r}) &= \frac{7}{8} \nabla^2 u_1(\vec{r}) \\ &+ \int K(\vec{r}' - \vec{r}) u_1(\vec{r}') d^2 r' + O(a) + o(u_1, u_2) \end{aligned} \quad (\text{B8})$$

is nonlocal. In polar coordinates $K(\vec{r}) = -(3/\pi)r^{-4} \cos 4\varphi$. These conclusions do not require a to be small, because the additional terms $O(a)$ depend on a and they can cancel the non-analyticity calculated here at most at particular values of a .

This transition from local basic equations to amplitude equations with *algebraically* decaying non-localities is counter-intuitive and misleading. This approach has the advantage that in Fourier space the linear dynamics (B5) is simple. This is useful for calculations of patterns stability involving only a few Fourier modes.

Finally, notice that a general method to reobtain local amplitude equations from the Fourier representation (B5), e.g. by redefining the amplitudes, should not be expected. Equation (B5) is general enough to include even non-local interactions in the basic equations, which certainly cannot lead to local amplitude equations.

3. The center manifold method

Alternatively, in the ‘‘center manifold’’ method only the slow modes at $\vec{q} = 0$, $V_j(0)$, are used for the characterization of the physical state

$$U(\vec{r}) = \sum_{j \in K} \int_{\Omega} u_j(\vec{q}) V_j(0) \exp(i\vec{q} \cdot \vec{r}) d\vec{q} + R(\{u_k\}). \quad (\text{B9})$$

The ‘‘slow subspace’’ spanned by the sum in Eq. (B9) can be extracted by the projection operator

$$P \cdot := \sum_{j \in K} P_j \cdot, \quad (\text{B10})$$

with

$$P_j f(\vec{r}) := \int_{\Omega} d\vec{q} \int \frac{d\vec{r}'}{(2\pi)^D} \langle W_j(0) | f(\vec{r}') \rangle V_j(0) \exp(i\vec{q} \cdot (\vec{r} - \vec{r}')), \quad (\text{B11})$$

where it is assumed without loss of generality that the states $W_j(0)$ and $V_j(0)$ ($j \in K$) entering P form a bi-orthonormal system. The ‘‘slaved’’ contributions $R(\{u_k\})$ cover the remaining subspace.

The factor $V_j(0)$ in Eq. (B9) can be pulled out of the integral, which is then simply the inverse Fourier transform of $u_j(\vec{q})$ into physical space $u_j(\vec{r})$. It is thus justified to define $u_j(\vec{r})$ as (the local average of) the hydrodynamic variable $\langle W_j | U(\vec{r}) \rangle$. In particular, if $\langle W_j | U(\vec{r}) \rangle$ is conserved, so is $u_j(\vec{r})$. In such a local representation, the vicinity of the ‘‘center manifold’’ method to a multiple scale approximation would be more obvious. Similar simplifications would also be possible for the integrals below, but have been suppressed in order to ease the comparison with the ‘‘order parameter’’ method.

The function $R(\{u_k\})$ is defined by the perturbative solution of

$$(1 - P)F(U) = 0, \quad (\text{B12})$$

where U is given by Eq. (B9) and the u_k are small and vary slowly and smoothly in space and time but are otherwise arbitrary.

At linear order in U , where Eq. (B12) reduces to

$$(1 - P)L(\partial_t, \nabla)U = 0, \quad (\text{B13})$$

a form

$$R(\{u_k\}) = \sum_{j \notin K} \int_{\Omega} r_j(\vec{q}) V_j(0) \exp(i\vec{q} \cdot \vec{r}) d\vec{q} \quad (\text{B14})$$

with contributions $r_j(\vec{q})$ only in the vicinity of $q = 0$ is sufficient.

The amplitude equations are then given by

$$P_i L(\partial_t, \nabla)U = 0 \quad \text{for each } i \in K \quad (\text{B15})$$

where R is eliminated from U via Eq. (B13).

When Eqs. (B13,B15) are satisfied with slowly varying u_k and small $R(\{u_k\})$, this implies that U contains no fast eigenvectors of $L(\partial_t, \nabla)$. Hence the resulting linear dynamics for U is the same as the one obtained with the ‘‘order parameter’’ method, in particular $R(\{u_k\})$ is then given by Eq. (B14) with

$$r_j(\vec{q}) = - \sum_{k,l} \langle W_k(\vec{q}) | V_j(0) \rangle^{-1} \langle W_k(\vec{q}) | V_l(0) \rangle u_l(\vec{q}), \quad (\text{B16})$$

where $l \in K$ is running over all fast modes and $j, k \notin K$ are running over all slow modes (for small $|\vec{q}|$ the matrix $\langle W_k(\vec{q}) | V_j(0) \rangle$ in this expression is generally a perturbed unit matrix and readily inverted).

To see that this method yields local dynamics for the amplitudes, split the linear operator, restricted to the subspace selected by $Q := (1 - P)$, like

$$Q L(\partial_t, \nabla) Q = \underbrace{Q L(0, 0) Q}_{:= L_0} + l(\partial_t, \nabla) \quad (\text{B17})$$

into a part L_0 which is regular, and a term which is small for slow temporal and spatial variations of the operand and polynomial in ∂_t, ∇ . Calling the sum on the r.s.h. of Eq. (B9) $S(\{u_k\})$, and suppressing the arguments (such that $U = S + R$), equation (B13) becomes

$$Q L R = Q L Q R = (L_0 + l) R = -Q L S, \quad (\text{B18})$$

and is solved by expanding for small l , i.e.

$$R = - \sum_{n=0}^{\infty} (-L_0^{-1} l(\partial_t, \nabla))^n L_0^{-1} Q L(\partial_t, \nabla) S. \quad (\text{B19})$$

When eliminating R from Eq. (B15) by Eq. (B19) and truncating at some power in the derivatives (i.e., for slow

enough variations), linear amplitude equations with local interactions are obtained. The extension to the nonlinear level is straightforward (s. Section V A).

It should be noticed that with this approach all modes in the kernel of $L(0, 0)$ have to be treated as “soft modes”, some of which, e.g. those resulting from gauge symmetries, may not actually have slowly relaxing modulations associated with them (see e.g. the pressure mode in Sec. IV B). For the simple example (B6) the “center manifold” method leads to amplitude equations identical to the basic equations.

The reason for the difference between the two approaches is that in the multidimensional kernel of $L(0, 0)$ the choice of the basis vectors characterizing the slow modes is not unique. While they are fixed (with respect to the hydrodynamic variables in the “microscopic equations”) for the “center manifold” method, they point, depending on \vec{q} , into arbitrary directions in the slow space for the “order parameter” method. For the same reason, there is no near identity transformation mapping one representation onto the other.

-
- [1] M. C. Cross and P. C. Hohenberg, *Rev. Mod. Phys.* **65**, 851 (1993).
- [2] K. Julien, E. Knobloch, and S. Tobias, *Physica D* **128**, 105 (1999).
- [3] K. Julien and E. Knobloch, *Phys. Fluids* **11**, 1469 (1999).
- [4] J. P. Keener, *Physica D* **31**, 269 (1988).
- [5] T. Frisch and S. Rica, *Physica D* **61**, 155 (1992).
- [6] M. Gabbay, E. Ott, and P. N. Guzdar, *Phys. Rev. Lett.* **78**, 2012 (1997).
- [7] O. Törnkvist and E. Schröder, *Phys. Rev. Lett.* **78**, 1908 (1997).
- [8] I. S. Aranson, A. R. Bishop, and L. Kramer, *Phys. Rev. E* **57**, 5276 (1998).
- [9] G. Rousseau, H. Chate, and R. Kapral, *Phys. Rev. Lett.* **80**, 5671 (1998).
- [10] W. Jahnke, C. Henze, and A. Winfree, *Nature* **336**, 662 (1988).
- [11] M. Vinson, S. Mironov, S. Mulvey, and A. Pertsov, *Nature* **386**, 447 (1997).
- [12] W. Pesch and U. Behn, in *Evolution of Spontaneous Structures in Dissipative Continuous Systems*, edited by F. H. Busse and S. C. Müller (Springer, New York, 1998), pp. 335–383.
- [13] L. Kramer and W. Pesch, in *Pattern formation in liquid crystals*, edited by A. Buka and L. Kramer (Springer, New York, 1995).
- [14] L. Kramer and W. Pesch, *Annu. Rev. Fluid Mech.* **27**, 515 (1995).
- [15] P. de Gennes and J. Prost, *The Physics of Liquid Crystals* (Clarendon Press, Oxford, 1993).
- [16] S. Chandrasekhar, *Liquid Crystals* (University Press, Cambridge, 1992).
- [17] R. Williams, *J. Chem. Phys.* **39**, 384 (1963).
- [18] E. Dubois-Violette, P. D. Gennes, and O. Parodi, *J. Phys. (Paris)* **32**, 305 (1971).
- [19] R. Ribotta and G. Durand, *J. Phys. (Paris) Colloque* **C3**, 334 (1979).
- [20] V. G. Chigrinov and S. A. Pikin, *Kristallografiya* **23**, 333 (1978).
- [21] M. I. Barnik, L. M. Blinov, S. A. Pikin, and A. N. Trufanov, *Zh. Èksper. Teoret. Fiz.* **72**, 756 (1977); translation in *Sov. Phys. JETP* **45**, 396 (1977).
- [22] M. Barnik, L. Blinov, M. Grebenkin, and A. Trufanov, *Mol. Cryst. Liq. Cryst.* **37**, 47 (1976).
- [23] M. Scheuring, L. Kramer, and J. Peinke, *Phys. Rev. E* **58**, 2018 (1998), calculations therein make use of viscosities at 20°C from [69] (priv. com.).
- [24] H. Amm, R. Stannarius, and A. G. Rossberg, *Physica D* **126**, 171 (1999).
- [25] P. Toth, A. Buka, J. Peinke, and L. Kramer, *Phys. Rev. E* **58**, 1983 (1998).
- [26] J.-H. Huh, Y. Hidaka, and S. Kai, *J. Phys. Soc. Jpn.* **68**, 1567 (1999).
- [27] W. Helfrich, *J. Chem. Phys.* **51**, 4092 (1969).
- [28] H. Pleiner and H. Brand, in *Pattern formation in liquid crystals*, edited by A. Buka and L. Kramer (Springer, New York, 1995), pp. 15–67.
- [29] H. R. Brand and H. Pleiner, *J. Phys. (Paris)* **45**, 563 (1984).
- [30] I. W. Smith *et al.*, *J. Phys. (Paris) Coll.* **36**, 237 (1975).
- [31] G. Dangelmayr and L. Kramer, in *Evolution of Spontaneous Structures in Dissipative Continuous Systems*, edited by F. H. Busse and S. C. Müller (Springer, New York, 1998), pp. 1–85.
- [32] W. Pesch and L. Kramer, in *Pattern formation in liquid crystals*, edited by A. Buka and L. Kramer (Springer, New York, 1995), pp. 69–90.
- [33] A. Lindner, Diploma thesis, Universität Bayreuth, 1997.
- [34] N. V. Madhusudana and V. A. Raghunathan, *Liq. Cryst.* **5**, 1789 (1989).
- [35] U. Schneider, M. de la Torre Juárez, W. Zimmermann, and I. Rehberg, *Phys. Rev. A* **46**, 1009 (1992).
- [36] E. Bodenschatz, W. Zimmermann, and L. Kramer, *J. Phys. (Paris)* **49**, 1875 (1988).
- [37] S. Kai and W. Zimmermann, *Prog. Theor. Phys. Suppl.* **99**, 458 (1989).
- [38] W. Thom, W. Zimmermann, and L. Kramer, *Liq. Cryst.* **4**, 309 (1989).
- [39] L. Kramer *et al.*, *Liquid Crystals* **5**, 699 (1989).
- [40] E. Plaut and W. Pesch, *Phys. Rev. E* **59**, 1747 (1999).
- [41] H. Haken, *Synergetics* (Springer, New York, 1978).
- [42] M. C. Cross, *Phys. Fluids* **23**, 1727 (1980).
- [43] A. C. Newell, T. Passot, and J. Lega, *Annu. Rev. Fluid Mech.* **25**, 399 (1993).
- [44] Q. Feng, W. Decker, W. Pesch, and L. Kramer, *J. Phys. France* **II 2**, 1303 (1992).
- [45] H. Mori and Y. Kuramoto, in *Dissipative Structures and Chaos* (Springer, New York, 1997), Chap. 5.
- [46] L. Y. Chen, N. Goldenfeld, and Y. Oono, *Phys. Rev. E* **54**, 376 (1996).
- [47] S. Chapman and T. G. Cowling, *The Mathematical Theory of Non-Uniform Gases*, 3rd ed. (Cambridge Univ.

- Press, London, 1970).
- [48] J.-P. Hansen and I. R. McDonald, in *Theory of simple liquids*, 2nd ed. (Academic Press, London, 1990), Chap. 8,9, and references therein.
- [49] N. G. van Kampen, *J. Stat. Phys.* **46**, 709 (1987).
- [50] Y. Kuramoto, in *Spatial inhomogeneities and transient behaviour in chemical kinetics*, edited by P. Gray *et al.* (Manchester University Press, Manchester, 1990), pp. 299–315.
- [51] P. Manneville, *Dissipative Structures and Weak Turbulence* (Academic Press, New York, 1990).
- [52] M. Ipsen, F. Hynne, and P. Sørensen, *Physica D* **136**, 66 (2000).
- [53] A. G. Rossberg and L. Kramer, *Phys. Scr.* **T67**, 121 (1996).
- [54] A. N. Trufanov, L. M. Blinov, and M. I. Barnik, *Zh. Èksper. Teoret. Fiz.* **78**, 622 (1980), translated in *Sov. Phys. JETP* **51**, 314 (1980).
- [55] S. Pikin and V. Chigrinov, *Sov. Phys. JETP* **51**, 123 (1980), original in *Zh.Èksp.Teor.Fiz.* **78**, 246 (January 1980).
- [56] A. G. Rossberg, A. Hertrich, L. Kramer, and W. Pesch, *Phys. Rev. Lett.* **76**, 4729 (1996).
- [57] L. Kramer and H. Zhao, priv. comm.
- [58] A. G. Rossberg, Dissertation, Universität Bayreuth, 1997, <http://www.rossberg.net/ag/dissertation>.
- [59] E. D. Siggia and A. Zippelius, *Phys.Rev.Lett.* **47**, 835 (1981).
- [60] A. C. Newell, T. Passot, and M. Souli, *J. Fluid Mech.* **220**, 187 (1990).
- [61] M. Kaiser and W. Pesch, *Phys. Rev. E* **48**, 4510 (1993).
- [62] H. Bohatsch and R. Stannarius, *Phys. Rev. E* **60**, 5591 (1999).
- [63] A. G. Rossberg, (2000), to appear in *Phys. Rev. E*, nlin/0004014.
- [64] E. Plaut *et al.*, *Phys. Rev. Lett* **79**, 2367 (1997).
- [65] A. G. Rossberg and L. Kramer, *Physica D* **115**, 19 (1998).
- [66] A. G. Rossberg, N. Éber, A. Buka, and L. Kramer, *Phys. Rev. E* **61**, R25 (2000).
- [67] J. T. Gleeson, N. Gheorghiu, and E. Plaut, pattsol/9907002, submitted to *Europhysics Letters* (unpublished).
- [68] L. M. Blinov and V. G. Chigrinov, *Electrooptic Effects in Liquid Crystal Materials* (Springer, New York, 1993).
- [69] H.-H.Graf, H.Kneppe, and F.Schneider, *Mol. Phys.* **77**, 521 (1992).
- [70] M. Treiber, N. Éber, Á. Buka, and L. Kramer, *J. Phys. II France* **7**, 649 (1997).

	MBBA ⁴ , 2 nd lowest;	4 th lowest Fourier approximation	Phase 5 ⁵ , 4 th lowest
E_c^2/ω	$7.52 \times 10^9 \text{ V}^2 \text{ s m}^{-2}$	$7.74 \times 10^9 \text{ V}^2 \text{ s m}^{-2}$	$4.01 \times 10^9 \text{ V}^2 \text{ s m}^{-2}$
q_c^2/ω	$1.53 \times 10^9 \text{ s m}^{-2}$	$1.79 \times 10^9 \text{ s m}^{-2}$	$1.19 \times 10^9 \text{ s m}^{-2}$
τ/τ_0	1.01	1.05	0.707
$q_c^2 \xi_x^2$	0.796	1.06	1.89
$q_c^2 \xi_y^2$	1.39 + ...	$1.41 - 0.0089e_-^2 + 0.0138e_-e_+ - 0.0032e_+^2 -$ $-0.0012e_- \zeta'^E + 0.0005e_+ \zeta'^E - 0.0004 \zeta'^E{}^2$	1.26 + ...
$q_c^2 \xi_z^2$	5.92 + ...	$6.00 - 0.0031e_+^2 + 0.0017e_+ \zeta'^E - 0.0014 \zeta'^E{}^2$	5.59
$q_c \beta_y$	$-q_c^2 \xi_y^2 + \dots$	$-q_c^2 \xi_y^2 + 0.0022e_-e_+ + 0.0045e_- \zeta'^E$	$-q_c^2 \xi_y^2 + \dots$
$E_c \alpha_x$...	$0.0216 e_+ + 0.0439 \zeta'^E$...
κ_x/τ_0	-0.445	-0.388	-0.690
κ_z/τ_0	$\sim \rho_m$	$6 \times 10^{-7} - 3.13 \times 10^{-9} \text{ m}^3 \text{ kg}^{-1} \rho_m$	
g	9.37 + ...	$9.39 + 0.0056e_+^2 - 0.0452e_+ \zeta'^E + 0.0755 \zeta'^E{}^2$	9.12 + ...
$I_r/E_c \omega \epsilon_\perp$	0.265	0.277	0.293
$I_i/E_c \omega \epsilon_\perp$	0.0408	0.0518	0.128
$q_c I_{rx}/E_c \omega \epsilon_\perp$	-0.0229 + ...	$-0.0312 + 6.21 \times 10^{-5} e_+^2 - 3.12 \times 10^{-5} e_+ \zeta'^E - 3.08 \times 10^{-5} \zeta'^E{}^2$	0.590 + ...
$q_c I_{ix}/E_c \omega \epsilon_\perp$	-0.459 + ...	$-0.451 - 1.00 \times 10^{-4} e_+^2 + 5.04 \times 10^{-5} e_+ \zeta'^E + 4.98 \times 10^{-5} \zeta'^E{}^2$	-0.502 + ...
$q_c I_{rz}/E_c \omega \epsilon_\perp$	0.7115	0.642	0.992
$q_c I_{iz}/E_c \omega \epsilon_\perp$	0.2254	0.250	0.671
$S_E/E_c^2 \epsilon_\perp$	0.0728	0.0851	0.162
Below this line, all values are given in units of 10^{-12} N .			
S_E/q_c^2	16.6	17.1	25.2
S_x/q_c^2	-2.23	-1.96	-3.56
S_z/q_c^2	6.14	7.49	18.2
S_{xx}/q_c	-7.34	-5.95	-16.4
S_{yy}/q_c	8.32 + ...	$7.07 + 0.0419 e_-^2 - 0.0561 e_- e_+ + 0.0141 e_+^2 +$ $+0.0017 e_- \zeta'^E - 0.0022 e_+ \zeta'^E - 1. \times 10^{-4} \zeta'^E{}^2$	10.1 + ...
S_{zz}/q_c	-17.6 + ...	$-15.7 + 0.0101 e_- e_+ - 0.0101 e_+^2 +$ $+0.0050 e_- \zeta'^E - 0.0052 e_+ \zeta'^E - 1. \times 10^{-4} \zeta'^E{}^2$	-5.49 + ...
S_{xy}/q_c	9.86 + ...	$8.66 - 0.0847 e_- \zeta'^E + 0.0285 e_+ \zeta'^E - 0.00500 \zeta'^E{}^2$	10.2 + ...
S_{xz}/q_c	-13.7 + ...	$-11.8 - 0.0201 e_+^2 - 0.0102 e_+ \zeta'^E - 1. \times 10^{-4} \zeta'^E{}^2$	0.317 + ...
S_{zx}/q_c	34.8	34.8	88.8
Γ	-14.6 + ...	$-14.5 - 0.557e_-^2 + 0.323e_-e_+ - 0.0565e_+^2 -$ $-0.195e_- \zeta'^E + 0.0665e_+ \zeta'^E - 0.0100 \zeta'^E{}^2$	-32.1 + ...

TABLE I. Coupling coefficients in the 3D dynamics of dielectric EC patterns at $\omega\tau_0 := \omega\epsilon_\perp/\sigma_\perp = 8$. The first column reproduces the analytic results Eqs. (A1-A21). The second and third column give accurate numerical results for MBBA and Phase 5 (Merck). For the units of the flexoelectric constants, see Appendix A. Ellipsis stand for suppressed flexoelectric contributions.

⁴Using the parameter set ‘‘MBBA I’’ from Ref. [36].

⁵As tabulated in Ref. [70] for 30°C, $\epsilon_\perp = 5.22 \epsilon_0$.

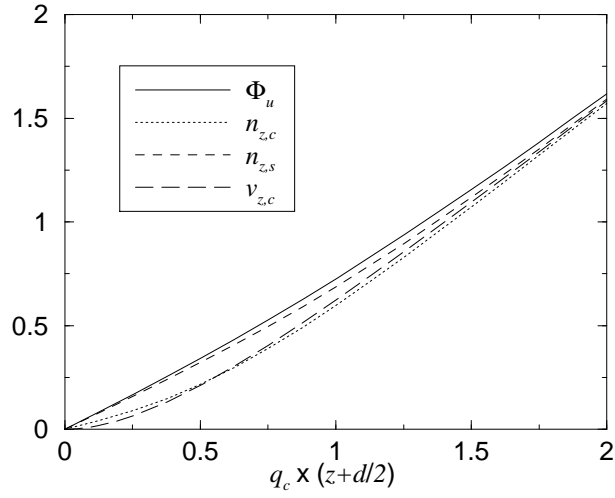


FIG. 1. Linear boundary layer calculated in the lowest Fourier approximation for MBBA. The temporally unmodulated component of the potential Φ_u , the in phase and out of phase components of the director tilt $n_{z,c}$, $n_{z,s}$, and the in phase component of the velocity $v_{z,c}$ are shown, normalization to unit slope at large distance ($\lambda \ll (z + d/2) \ll d$) from the boundaries.

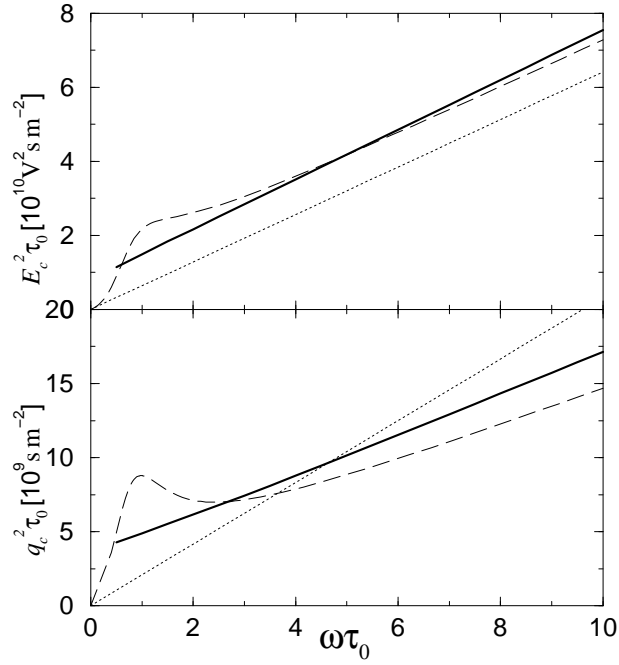


FIG. 2. $E_c^2 \tau_0$ and $q_c^2 \tau_0$ calculated for MBBA, including Fourier modes up to ω (dotted), 2ω (dashed), and 7ω (solid).